

Chapter 2

Coherent Optical Techniques

The emergence of coherent light sources stimulated a qualitative jump in the evolution of experimental mechanics techniques. Pioneering works in this field appeared in the 1960s (Leith and Upatnieks [21]; Denisyuk [22]). However, by 1980 the original methods for SSS analysis based on coherent optics, *holographic interferometry*, were used widely not only at academic scientific centers but also at design institutes and factory laboratories when elaborating and constructing emerging technologies. Unrivalled opportunities for no-touch obtaining high-precision information about the SSS of the objects under static, vibrational, and dynamic loads offered by holographic interferometry, *speckle metrology*, and, especially, *electronic correlation speckle pattern interferometry* and *digital holography* emerged at a later date to allow coherent optical methods to be considered as the most important and promising direction of experimental mechanics of deformable solids [4, 23–27 and others]. The correct interpretation of primary information in the language of those physical magnitudes (the recording of which is an objective of the experiment) remains the central problem arising in practical application of these methods.

2.1 Holographic Interferometry

Holography is the mode for recording and reconstructing optical waves based on recording intensity distribution in an interference pattern (hologram) formed by reference and object waves. The foundations of holography were created by Gabor [28] who proposed a way for recording not only amplitude, but also phase information about electronic waves by means of imposition of a coherent reference wave. At that time, however, his ideas did not find practical use due to the lack of powerful sources of coherent radiation.

The term “holographic interferometry” unites a broad range of special optical methods for studying different characteristics of physical objects’ state or behavior through interference comparison of coherent light waves reflected by body surface. Here a common principle for all particular approaches is the fact that coincidence in time and interference of the waves containing, in the general case, information about

the states of the “object-measuring instrument” system at different points of time are provided by their consecutive recording at holograms with subsequent simultaneous reproduction (reconstruction).

The basic principles of holography used in experimental mechanics are considered below.

2.1.1 Theoretic Framework of Interference Pattern Formation

2.1.1.1 Holography by Double-Exposure Holographic Interferometry

Let us consider the process of image formation according to the schematic shown in Fig. 2.1. In this procedure (proposed for the first time by Leith and Upatnieks [21]) the off-axis reference beam is used to obtain a hologram by *double-exposure*

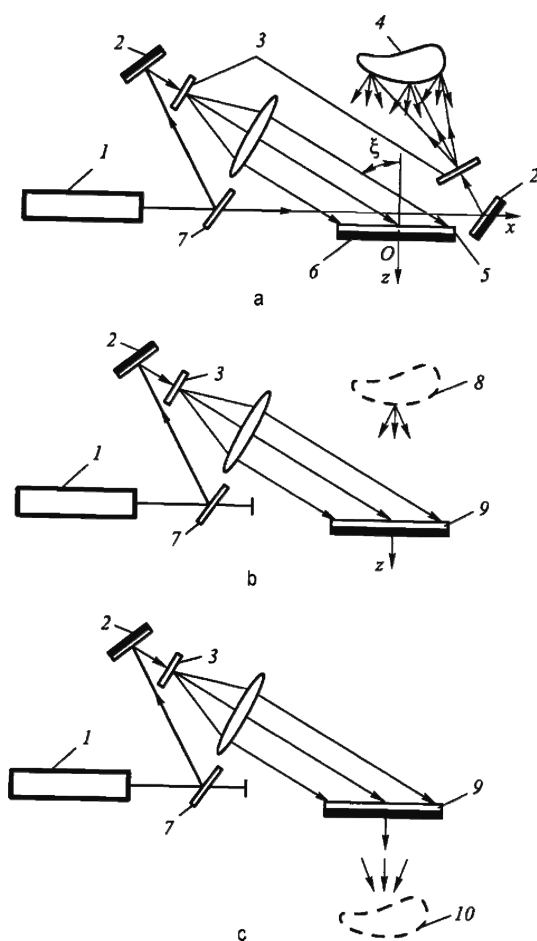


Fig. 2.1 Schematics of double-exposure holographic interferometry: (a) optical schematic for hologram recording; (b), (c) recovery of virtual and real image, respectively; 1 – laser; 2 – mirror; 3 – microscope objective; 4 – object; 5 – photoemulsion; 6 – photographic plate; 7 – beam splitter; 8 – virtual image; 9 – hologram; 10 – real image

holographic interferometry. The light beam reflected by a body to the hologram plane can be described by the following expression,

$$E = \text{Re} [B \exp(i\varphi)], \quad (2.1)$$

where $B(x, y)$, $\varphi(x, y)$ are the amplitude and phase of the light wave, and both magnitudes are, in general, case functions of point coordinates in the hologram plane.

The reference beam of the light whose source is high coherent laser radiation can be presented in the form of a plane wave with amplitude A not depending on Cartesian coordinates x and y (plane Oxy coincides with the hologram plane; axis Oz is perpendicular to it). As Leith and Upatnieks had shown, the plane wave perpendicular to axis Oy and characterizing the reference beam incident at angle ξ to axis Oz is described in the hologram plane by expression:

$$E_R = \text{Re}\{A \exp(i2\pi/\lambda)x \sin \xi\}, \quad (2.2)$$

where $(2\pi/\lambda)x \sin \xi$ is the phase shift. It should be noted that in expression (2.2) amplitude A is a real part of the complex function.

Two exposures of the object being considered are carried out in the method under consideration: the first exposure for its specific initial (nonloaded) condition and the second for the loaded (deformed) state.

For the first exposure total illumination in the hologram plane represents the superposition of two wavefronts: the beam reflected from the object and the reference wave; that is,

$$E_1 = E_{01} + E_R. \quad (2.3)$$

For the second exposure we can write by analogy,

$$E_2 = E_{02} + E_R. \quad (2.4)$$

The magnitude E_R is the same for both exposures; amplitude E_{01} is given by expression (2.1), and E_{02} can be expressed as

$$E_{02} = \text{Re}\{B \exp[i(\varphi + \Delta\varphi)]\}, \quad (2.5)$$

where $\Delta\varphi(x, y)$ is the change in wave phase due to displacement of the object surface. It should be noted that expression (2.5) is true only for relatively small displacements.

It is known from physics that total exposure I in the photographic emulsion plane after the exposure process is determined by correlation

$$I = |E_{01} + E_R|^2 t_1 + |E_{02} + E_R|^2 t_2, \quad (2.6)$$

where t_1, t_2 are the times of the first and second exposure processes, respectively.

Let us determine I for the case $t_1 = t_2 = t$. Having substituted correlations (2.1)–(2.5) into expression (2.6) and denoted $\gamma = (2\pi/\lambda)x \sin \xi$ we obtain

$$\begin{aligned} I/t &= [B \exp(i\varphi) + A \exp(i\gamma)][B \exp(-i\varphi) + A \exp(-i\gamma)] \\ &\quad + \{B \exp[i(\varphi + \Delta\varphi)] + A \exp(i\gamma)\}\{B \exp[-i(\varphi + \Delta\varphi)] + A \exp(-i\gamma)\} \\ &= 2(A^2 + B^2) + AB \exp(i\gamma)\{\exp(-i\varphi) + \exp[-i(\varphi + \Delta\varphi)]\} \\ &\quad + AB \exp(-i\gamma)\{\exp(i\varphi) + \exp[i(\varphi + \Delta\varphi)]\}. \end{aligned} \quad (2.7)$$

Expression (2.7) describes illumination in the course of hologram recording according to double-exposure holographic interferometry. The displacement of the object being studied can be judged by phase change $\Delta\varphi$.

2.1.1.2 Image Reconstruction from Hologram

Photographic properties of a photographic plate are described by the so-called characteristic curve [4, 25] that represents a dependence of *degree of blackening* Ω upon the exposure logarithm I (Fig. 2.2a). The slope of the characteristic curve determines the *degree of contrast* χ .

When describing the holographic process, the properties of a photographic plate can be presented as a dependence of photolayer *amplitude transmission* $T = \sqrt{\tau}$ upon exposure I (Fig. 2.2b), where τ is the transmission coefficient of the developed layer, $\lg(1/\tau) = \Omega$. As a rule, dependence $T(I)$ is approximated by the right line:

$$T = b_0 + b_1 I.$$

where b_0, b_1 are coefficients.

To reconstruct the fixed image at the twice-exposed hologram the processed photographic plate is placed according to the holographic schematics presented in Fig. 2.1b,c.

Illuminating the twice-exposed hologram by the reference beam a new wave originates whose amplitude E_{pr} is proportional to transmission coefficient T . For the wave passed through the hologram it can be written:

$$E_{pr} = TE_R = (b_0 + b_1 I)A \exp(-i\gamma)$$

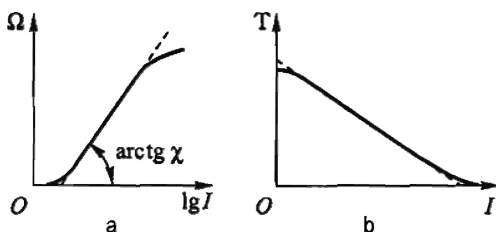


Fig. 2.2 Characteristic curve of photographic layer (a) and dependence of amplitude transmission upon exposure (b)

Taking into account correlation (2.7) we obtain

$$\begin{aligned}
 E_{\text{pr}} = & [b_0 + 2b_1t(A^2 + B^2)]A \exp(i\gamma) \\
 & + A^2Bb_1t\{\exp(-i\varphi) + \exp[-i(\varphi + \Delta\varphi)]\} \\
 & + A^2Bb_1t\{\exp(i\varphi) + \exp[i(\varphi + \Delta\varphi)]\} \exp(2i\gamma).
 \end{aligned} \tag{2.8}$$

Let us analyze expression (2.8). The first summand represents within the accuracy of constant $b_0 + 2b_1t(A^2 + B^2)$ the amplitude of the reference wave passed through the hologram, the second summand describes within the accuracy of the real multiplier b_1tA^2B , two object waves forming a virtual image, and, finally, the third summand corresponds to the distorted (influence of the comultiplier $\exp(2i\gamma)$) real image.

The illumination distribution for a virtual image will correspond to the square of the second summand in expression (2.8):

$$\begin{aligned}
 I_{\text{virt}} = & A^4B^2b_1^2t^2\{\exp(-i\varphi) + \exp[-i(\varphi + \Delta\varphi)]\}^2 \\
 = & I'\{1 + \exp[-i(\varphi + \Delta\varphi)]\exp(i\varphi) + \exp[i(\varphi + \Delta\varphi)]\exp(-i\varphi) + 1\} \\
 = & I'[2 + \exp(-i\Delta\varphi) + \exp(i\Delta\varphi)] = 2I_0(1 + \cos \Delta\varphi).
 \end{aligned}$$

Consequently

$$I_{\text{virt}} = 2I'(1 + \cos \Delta\varphi), \tag{2.9}$$

where $I' = A^4B^2b_1^2t^2$. It should be noted that the wavelength of the radiation source used for hologram reconstruction need not be the same as for its recording, however, the requirement for their coherence remains.

Expression (2.9) is a basic correlation of double-exposure holographic interferometry. The interference fringes are the geometric locus of the points where the intensity of the virtual image is equal to zero; that is, the following condition is fulfilled,

$$1 + \cos \Delta\varphi = 2 \cos^2(\Delta\varphi/2) = 0, \tag{2.10}$$

and serves as initial information used to obtain displacement fields for the object being studied.

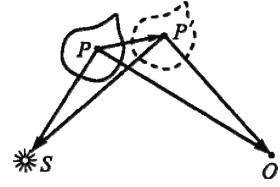
2.1.1.3 Change in Phase with Body Straining

The phase change $\Delta\varphi$ conditioned by displacement of the object surface between two exposures is associated with the change in length of the light optical path. To analyze the interference pattern process with object straining let us consider the schematic presented in Fig. 2.3.

As shown in Fig. 2.3 the length of the light optical path corresponding to the first exposure (the undeformed state of the object) is

$$L_1 = |PS| + |PO|. \tag{2.11}$$

Fig. 2.3 Schematic of interference fringe formation during body straining (S is the light source, P is an arbitrary point at the body surface, and O is a point in the hologram plane)



Using the scalar product of the vectors, correlation (2.11) can be rewritten in the form

$$L_1 = \sqrt{(PS \cdot PS)} + \sqrt{(PO \cdot PO)} \quad (2.12)$$

During body straining point P draws to point P' . For the deformed body state the length of the light optical path

$$L_2 = |P'S| + |P'O|. \quad (2.13)$$

Let us express length difference $L_1 - L_2$ in terms of the change in phase of the light wave:

$$\Delta\varphi = \frac{2\pi}{\lambda} (L_1 - L_2). \quad (2.14)$$

For the convenience of further inferences (and practical computations) let us write down evident correlations:

$$PS = PP' + P'S, \quad PO = PP' + P'O. \quad (2.15)$$

After substitution of correlation (2.15) in (2.12) we obtain

$$L_1 = \sqrt{|P'S|^2 + 2|P'S| \cdot |PP'| (p's \cdot pp') + |PP'|^2} \\ + \sqrt{|P'O|^2 + 2|P'O| \cdot |PP'| (p'o \cdot pp') + |PP'|^2},$$

where $p's$, $p'o$, and pp' are the unitary vectors of the corresponding vectors.

Having omitted the small quantity $|PP'|^2$ we write

$$L_1 = |P'S| \sqrt{1 + 2(p's \cdot pp') \frac{|PP'|}{|P'S|}} \\ + |P'O| \sqrt{1 + 2(p'o \cdot pp') \frac{|PP'|}{|P'O|}}. \quad (2.16)$$

Expanding expression (2.16) into Taylor series on small series expansion parameters, that is, $|\mathbf{PP}'|/|\mathbf{P'S}| \rightarrow 0$ and $|\mathbf{PP}'|/|\mathbf{P'O}| \rightarrow 0$, we find

$$L_1 = |\mathbf{P'S}| + |\mathbf{PP}'| (\mathbf{p's} \cdot \mathbf{pp'}) + |\mathbf{P'O}| + |\mathbf{PP}'| (\mathbf{p'o} \cdot \mathbf{pp'}). \quad (2.17)$$

Substituting correlations (2.17) and (2.13) into (2.14) we have

$$\begin{aligned} \Delta\varphi &= \frac{\lambda}{2\pi} (L_1 - L_2) = |\mathbf{PP}'| (\mathbf{p's} \cdot \mathbf{pp'}) + |\mathbf{PP}'| (\mathbf{p'o} \cdot \mathbf{pp'}) \\ &= |\mathbf{PP}'| [(\mathbf{p's} \cdot \mathbf{pp'}) + (\mathbf{p'o} \cdot \mathbf{pp'})] = |\mathbf{PP}'| [(\mathbf{p's} + \mathbf{p'o}) \cdot \mathbf{pp'}]. \end{aligned}$$

Because $\mathbf{p's} \approx \mathbf{ps}$ and $\mathbf{p'o} \approx \mathbf{po}$ we finally obtain

$$\Delta\varphi = \frac{2\pi}{\lambda} |\mathbf{PP}'| [(\mathbf{ps} + \mathbf{po}) \cdot \mathbf{pp'}]. \quad (2.18)$$

It should be noted that vector $(\mathbf{ps} + \mathbf{po})$ is referred to as the *vector of system sensitivity*.

Taking into account correlation (2.18) expression (2.9) acquires the form:

$$I_{\text{virt}} = 2I_0 \left\{ 1 + \cos \frac{2\pi}{\lambda} |\mathbf{PP}'| [(\mathbf{p's} + \mathbf{p'o}) \cdot \mathbf{pp'}] \right\}. \quad (2.19)$$

For the convenience of the practical application of Eq. (2.19) in determining displacements of points at the surface of the object being studied let us introduce the local Cartesian coordinate system associated with point P (Fig. 2.4). The vector of displacements we present as

$$\mathbf{pp'} = u_i \mathbf{e}_i, \quad i = 1, 2, 3,$$

where u_i is the displacement in the i th direction and \mathbf{e}_i are the unitary vectors in the directions of coordinate axes Px_1 , Px_2 , and Px_3 (see Fig. 2.4).

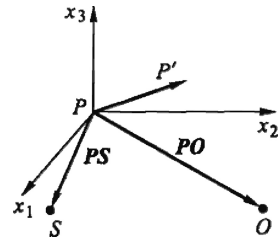


Fig. 2.4 Local orthogonal system of coordinates

Assume that unitary vectors \mathbf{ps} and \mathbf{po} are met by the set of direction cosines l_i and m_i , respectively. Then formula (2.19) can be written as

$$I_{\text{virt}} = 2I' \left[1 + \cos \frac{2\pi}{\lambda} (l_i u_i + m_i v_i) \right]. \quad (2.20)$$

Thus, the information derivable from the virtual (or real) image is connected with three components of displacement vector \mathbf{pp}' . Ennos [29] and Solid [30] have shown that if the fringes of zero order can be identified at the surface then for unambiguous determination of the displacement vector it is sufficient to obtain three holograms. In the cases when for one reason or another the determination of zero-order fringes is impossible, the one-hologram Aleksandrov–Bonch–Bruevich method should be used [31].

2.1.2 Measurement of Mechanical Vibrations

The measurement of mechanical oscillations is one of the most interesting and practically important application fields of holographic interferometry. The first work in this field was carried out by Powell and Stetson [32]. The essence of the method stated below is that the time-averaged complex amplitude of the light wave scattered by the object and incident at the hologram is recorded at the hologram. When object oscillations are described by a periodic function the object is near two positions of maximum displacement in which its velocity is equal to zero most of the time. Therefore the time-averaged holographic interferogram of the object is similar to the double-exposure hologram in which the fringes associated with its displacement between two extreme positions are fixed. As for the quantitative interpretation of such an interferogram the special analysis presented in the sequel is needed.

Let us consider a console plate (Fig. 2.5a) oscillating continuously about the middle position (Oxy is the middle plane of the plate) with natural frequency ω .

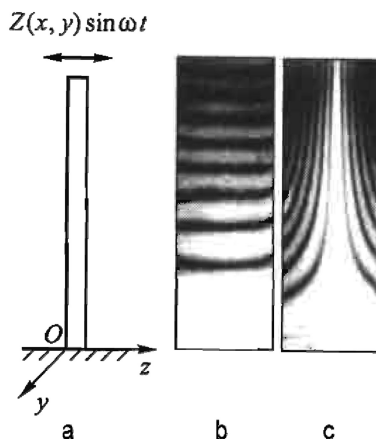


Fig. 2.5 Sine oscillations of console plate (a) schematic of plate fixing and direction of oscillations; (b), (c) interference patterns corresponding to oscillations at the first and second natural frequencies

Displacement of points of plate surfaces occurs in the axis Oz direction. The plate is illuminated by the plane wave of coherent radiation also propagating in the Oz direction; that is,

$$z(x, y, t) = Z \sin \omega t, \quad (2.21)$$

where $Z(x, y)$ is the amplitude of plate oscillations.

Let

$$E_{st} = B \exp(i\varphi) \quad (2.22)$$

be the complex amplitude of light scattered by the plate when it is motionless. Then the light passes a certain distance l_0 from the radiation source to the surface point.

During vibrations of the object the distance from the radiation source to the surface point constitutes $l_0 - 2Z \sin \omega t$. The corresponding change in the object wave phase in the plane of hologram is

$$\Delta\varphi(x, y, t) = \frac{2\pi}{\lambda} 2Z \sin \omega t, \quad (2.23)$$

and its amplitude is

$$E(x, y, t) = B \left[i \left(\varphi + \frac{4\pi}{\lambda} Z \sin \omega t \right) \right].$$

The method of time averaging lies in the fact that the hologram is recorded under the simultaneous effect of the object wave and off-axis reference wave on a photographic plate for time T .

After photographic treatment the hologram obtained in such a manner is illuminated by a reference wave. The amplitude for a reconstructed virtual image will be proportional to the value $E_0(x, y, t)$ averaged over the exposure time:

$$\begin{aligned} E &= \frac{1}{T} \int_0^T B \exp \left[i \left(\varphi + \frac{4\pi}{\lambda} Z \sin \omega t \right) \right] dt \\ &= E_{st} \frac{1}{T} \int_0^T \exp \left(i \frac{4\pi}{\lambda} Z \sin \omega t \right) dt = E_{st}(x, y) M_T \end{aligned} \quad (2.24)$$

The function

$$M_T = \frac{1}{T} \int_0^T \exp \left(i \frac{4\pi}{\lambda} Z \sin \omega t \right) dt \quad (2.25)$$

is known as the *characteristic fringe function* of sine oscillation.

Therefore, for the reconstructed virtual image the illumination is proportional to the square of amplitude:

$$I(x, y) = |E|^2 |M_T|^2 = B^2 \exp^2(i\varphi) |M_T|^2 = B^2 |M_T|^2. \quad (2.26)$$

If assumed exposure time is more essential than the oscillation period ($T \gg 1/\omega$) then for sine oscillations the characteristic function can be easily calculated

$$M_T = \lim_{T \rightarrow \infty} \frac{1}{T} \int_0^T \exp\left(i \frac{4\pi}{\lambda} Z \sin \omega t\right) dt = J_0 \frac{4\pi}{\lambda} Z, \quad (2.27)$$

where $J_0(x, y)$ is the zero-order Bessel function of the first kind.

The illumination obtainable in this case is proportional to the square of the function:

$$I(x, y) = B^2 J_0^2 \frac{4\pi}{\lambda} Z. \quad (2.28)$$

It follows from (2.28) that the virtual image reconstructed after illumination of the hologram by a reference wave is modulated by the system of fringes described by the square of the zero-order Bessel function of the first kind (Fig. 2.6). It means that the centers of dark fringes correspond to the points of the object of which the amplitude of $Z(x, y)$ vibrations is such that function $J_0(x, y) = 0$; that is,

$$J_0 \frac{4\pi}{\lambda} Z = 0. \quad (2.29)$$

The values of arguments ξ_n of Bessel function J_0 corresponding to its first 12 zeros are given in Table 2.1.

Let us determine amplitude displacements for the points of the plate surface placed at the fifth ($n = 5$) dark fringe (see Fig. 2.5b,c). According to the data of Table 2.1

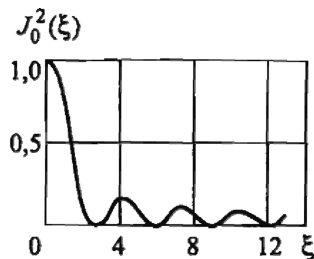


Fig. 2.6 Graph of function $J_0^2(\xi)$

Table 2.1 Values of arguments ξ_n corresponding to zeros of Bessel function J_0

n	ξ_n
1	2.4048
2	5.5200
3	8.6537
4	11.7915
5	14.9309
6	18.0710
7	21.2116
8	24.3524
9	27.4934
10	30.6346
11	33.7758
12	36.0170

$$\xi_5 = \frac{4\pi}{\lambda} Z_5 = 14.9309;$$

that is, amplitude displacements of these points $Z_5 = 14.9309 \cdot 4\pi/\lambda = 1.188\lambda$.

Thus, with application of the time-averaging method the intensity distribution in the interference fringes originating during the object sine oscillations is proportional to J_0^2 . It means that with an increase in the order of the fringe its luminance falls. The identification of zero-order fringe causes no difficulties inasmuch as it is much denser (see Fig. 2.6)

If the displacement of all object points is described by the same time function $F(t)$ then the characteristic function can be written as

$$M_T = \frac{1}{T} \int_0^T \exp \{i [\Delta\varphi_a F(t)]\} dt, \quad (2.30)$$

where $\Delta\varphi_a(x, y)$ is the amplitude phase shift of the light wave in the hologram plane.

The distribution of interference fringes (their illumination) at the virtual image reconstructed by the hologram is described by expression

$$I = M_T |\mathbf{K} \cdot \mathbf{B}|^2 = \left| \frac{1}{T} \int_0^T \exp[i(\mathbf{K} \cdot \mathbf{B})F(t)] dt \right|^2, \quad (2.31)$$

where \mathbf{K} is the sensitivity vector, $\mathbf{K} = \mathbf{ps} + \mathbf{po}$, and \mathbf{B} is the vector of motion amplitude for object points.

Correlation (2.31) is true for any form of time function $F(t)$. In particular, the following time function corresponds to the classical double-exposure holographic interferometry method.

$$F(t) = \begin{cases} 0 & \text{при } 0 \leq t < T/2 \\ 1 & \text{при } T/2 \leq t \leq T \end{cases} . \quad (2.32)$$

Let us determine the characteristic function for this case

$$M_T = \frac{1}{T} \int_0^{T/2} dt + \frac{1}{T} \int_{T/2}^T \exp[i(\mathbf{K} \cdot \mathbf{B})] dt = \frac{1 + \exp[i(\mathbf{K} \cdot \mathbf{B})]}{2}.$$

Therefore, at the virtual image reconstructed by the hologram

$$I = |M_T|^2 = \frac{1 + \cos(\mathbf{K} \cdot \mathbf{B})}{2} = \cos^2 \frac{(\mathbf{K} \cdot \mathbf{B})}{2}. \quad (2.33)$$

If we have a priori information about the form of function $F(t)$, the characteristic function M_T can be calculated on the basis of expression (2.30) at all times. But if the displacement of all object points represents multimode oscillatory motions then interpretation of the interference fringe pattern is a rather complicated problem. At the same time application of present-day mathematical operations together with automated processing of two-dimensional information enables obtaining quite correct solutions for problems of this class.

The holographic interferometry method is widely used in practice to analyze natural (resonance) oscillations of construction components. Natural frequencies of oscillations are determined by means of real-time holographic imaging of an object. As a rule, experimental procedures for measuring main vibration characteristics are two-stage.

At the first stage holographic imaging of an object is carried out under initial (stationary) conditions. After photochemical treatment and drying the photographic plate is returned to the same position coinciding exactly with the position occupied by it during hologram recording (to this effect special kinematical reset devices of various types are applied). Now the reference wave plays the role of reconstructing wave. As a consequence the waveforming, in particular, a virtual image of the object is reproduced. Also the wave is diffusively reflected by the surface of the real object and passed through the developed photographic plate which propagates after the hologram. If no variations occur from the time of the hologram recording then the components of both waves will be identical. Interference of these waves will consist only in the simple adding of their intensities. However, any subsequent phase transformations of the real reference wave will lead to the occurrence of an appropriate phase difference and, as a consequence, to the occurrence of a secondary interference structure characterizing the dynamics of occurring variations. Depending on the essence of the specific research task the fringe pattern is either observed visually or fixed with the help of some sort of physical detector: a photographic camera or video camera, among others.

For the determination of natural frequencies an additional linear phase shift of the illuminating wave is introduced into the optical arrangement. Such a shift can

be created by the turn of a light beam through the introduction of a glass plate placed at a specific small angle in the optical arrangement. With a motionless object or with the excitation frequencies differing appreciably from any of their natural frequencies, the interference pattern observed will represent a system of rectilinear fringes: carrier raster (in the strict sense, carrier fringes are rectilinear only at the plain surface of an object). For illustrative purposes such an interferogram fixed at the resting object—a cantilever fitted turbine bucket—is shown in Fig. 2.7a.

During scanning of a given range of excitation frequencies and occurrence of resonance effects the carrier fringes will disappear everywhere apart from the vicinity of nodal lines. The closer the excitation frequency is to the natural frequency of the object the smaller the size of the regions will be with the saved carrier structure of fringes. This fact enables one to fix the values of natural frequencies with sufficient precision and already at this stage to estimate the vibration mode according to the nodal line configuration. So, the interferogram presented in Fig. 2.7b and derived by the method described corresponds to the flexural vibration mode of the bucket with two horizontal and two vertical nodal lines.

At the second stage of the experiment the oscillation amplitude interference fringes are recorded at fixed frequencies using the time-averaging method. In Fig. 2.7c the interference fringes of equal oscillation amplitudes of the turbine bucket are shown; these fringes are fixed at the same excitation frequency as the fringes presented in Fig. 2.7b. Here the most luminous interference fringes correspond to nodal lines. For quantitative interpretation of the derived fringes the data presented in Table 2.1 are used. Some typical interferograms obtained during research into vibration modes of a cantilever cylindrical shell are presented in Fig. 2.8.

In conclusion it should be noted that the advantages of holographic interferometry in the tasks of vibrometry are evident in analyzing offbeat vibration modes for complicated constructions when interpretation of the data derived by conventional methods can involve certain difficulties. In addition, application of no-touch research methods is justified for tests of small-scale specimens when the standard sensors fastened onto them for recording one or another vibration parameter even having a very small mass produce appreciable distortions of the actual picture of object behavior.

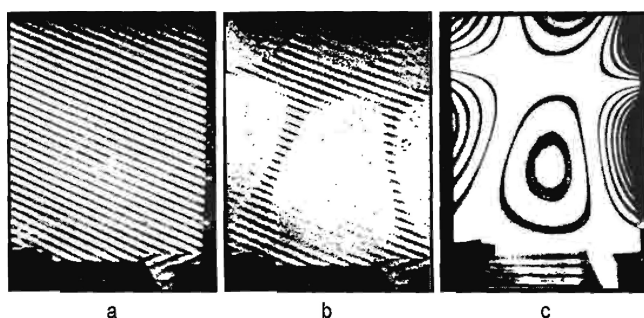
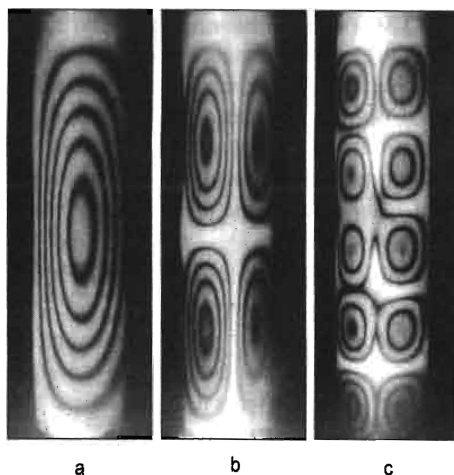


Fig. 2.7 Typical patterns of interference fringes observed during determination of the main vibration characteristics of objects

Fig. 2.8 Interference patterns corresponding to the first three oscillation frequencies



2.1.3 Certain Peculiarities of Holographic Interferometry Technique

Let us formulate the basic facts that have to be assimilated in order to understand the peculiarities of the holographic interferometry method.

1. The holographic platform should be mounted in such a manner that relative displacements of its components will not exceed $\lambda/4$ (using a helium–neon laser it constitutes $\sim 0.15 \mu\text{m}$). Building vibrations passing through the optical table are most commonly responsible for the relative displacement of holographic system components. For this reason the table should have sufficiently great mass and, as a rule, should be equipped with a vibration isolation system.
2. The detail surface being studied should be diffusively reflecting.
3. Accuracy in the relative position of holographic system components is not critical.
4. In principle the holograms can be recorded with any photographic emulsions for which resolution ability and sensitometric characteristics meet the study purpose. Usually the type of holographic plate is associated with the wavelength of the laser used. As a rule, for holograms recording at high resolution, emulsions of minute silver halide crystals ($0.4 \mu\text{m}$) deposited at glass plates are applied.

2.2 Speckle Photography

The basic advantage of speckle photography over other coherent optical techniques for measuring parameters of the deformed state are simplicity of optical arrangement, as well as presentation and interpretation of obtainable results. This method

can be used for measuring tangential displacements of surface of the object being studied and also for research into vibration processes, and so on [4, 23, 24, 33–35 and others]. Below we concentrate on the application of speckle photography for determining only tangential displacements of the surface being studied.

2.2.1 Laser Speckle Pattern

It is known from linear optics that each point of a wavefront can be considered as a separate source of light oscillations (Huygens' principle). In addition, a wave disturbance in any point of space can be considered as a result of interference of secondary waves from the fictive sources into which the wavefront is divided, and also the fictive sources can interfere in any point of space (Fresnel's principle).

If studying or photographing a diffusively reflecting or transmitting object in laser radiation, the image obtained appears grainy (Fig. 2.9). It seems that the surface of the object is coated by a host of little, chaotically situated, light and dark speckles.

Let us consider the physical nature of the speckles. Each point of the surface scatters light in the direction of the observer. Accordingly Fresnel's principle of highly coherent laser radiation scattered by one of the surface points interferes with the radiation scattered by other points of the object leading to the occurrence of a chaotic interference structure, that is, speckles. Their chaotic character is associated with surface roughness, in consequence of which the scattered light phase varies point-to-point in a random manner in accordance with the change in height of the surface microrelief. Bringing the eye or optical instrument to focus at the point placed in front of the object, the speckle pattern will continue to remain visible. With a change in observer position in relation to the object the speckle pattern is also displaced.

The speckle pattern recordable in the plane situated at a distance l_0 from the diffuser originates owing to superposition of interference patterns arising under light scattering by each pair of points at the diffuser.

First let us examine the interference pattern formed by two arbitrary points 1 and 2 situated at a distance b (Fig. 2.10). The opaque screen I is exposed to light by point source S situated at a distance l_s from the screen and displaced for short distance y_s from the symmetry axis of the system. The light diaphragm of two holes (or slits) forms an interference pattern that can be observed at the screen II remote from screen I with the holes for distance l .

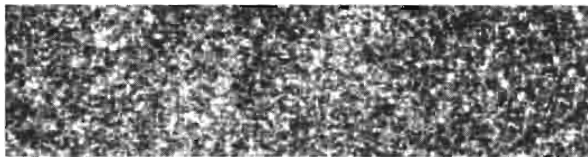


Fig. 2.9 Typical speckle pattern

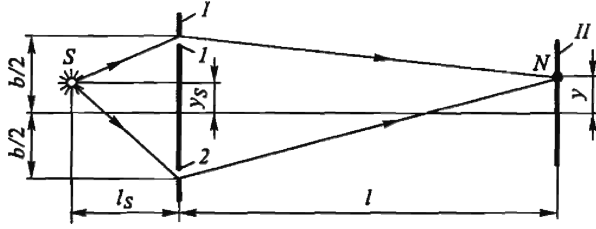


Fig. 2.10 Schematic of the simplest interferometer

Expression determining illumination of screen *II* in arbitrary point *N* has the form:

$$I = A_1^2 + A_2^2 + 2\sqrt{A_1^2 A_2^2} \cos \delta, \quad (2.34)$$

where A_1 and A_2 are the amplitudes of the light waves coming from holes 1 and 2, respectively ($I_1 = A_1^2$, $I_2 = A_2^2$) and δ is the phase difference between two waves arriving at point *N*.

In the case under consideration $\delta = (2\pi/\lambda)\Delta l$ where Δl is the path difference of the waves coming from source *S* to point of observation *N*.

Because y , y_s , and b are much less than l_s and l_o the illumination being created by each light wave in point *N* is approximately equal; that is, $I_1 \approx I_2 \approx I_0$. Taking this into consideration we obtain

$$I = I_0 + I_0 + 2\sqrt{I_0^2} \cdot \cos \delta = 4I_0 \cos^2(\delta/2). \quad (2.35)$$

According to Fig. 2.10,

$$\begin{aligned} \Delta l &= \left[\sqrt{l_s^2 + (b/2 - y_s)^2} + \sqrt{l_0^2 + (b/2 - y)^2} \right] \\ &\quad - \left[\sqrt{l_s^2 + (b/2 + y_s)^2} + \sqrt{l_0^2 + (b/2 + y)^2} \right] \\ &= l_s \left[\sqrt{1 + (b/2 - y_s)^2/l_s^2} - \sqrt{1 + (b/2 + y_s)^2/l_s^2} \right] \\ &\quad + l \left[\sqrt{1 + (b/2 - y)^2/l^2} - \sqrt{1 + (b/2 + y)^2/l^2} \right] \end{aligned}$$

By also taking into account that at $\varepsilon \ll 1$ correlation $(1 \pm \varepsilon)^{1/2} \approx 1 \pm \varepsilon/2$ we have

$$\Delta l = - \left(\frac{b y_s}{l_s} + \frac{b y}{l} \right). \quad (2.36)$$

With (2.36) expression (2.35) takes on form

$$I = 4I_0 \cos^2 \left[\frac{\pi b}{\lambda} \left(\frac{y_s}{l_s} + \frac{y}{l} \right) \right]. \quad (2.37)$$

It follows from expression (2.37) that $I = 0$ if

$$\frac{\pi b y}{\lambda l} = \frac{\pi}{2} + k\pi. \quad (2.38)$$

Equation (2.38) describes parallel Young's fringe spaced at intervals of $\lambda l/b$.

2.2.2 Evaluation of Speckle Width

For a quantitative description of the speckle pattern originating during laser light scattering by a diffusively reflecting surface the most important statistical characteristic of the speckles is speckle size. Let us assume that the speckle pattern is created with a uniformly illuminated diffuser of width B (Fig. 2.11). For simplicity of analysis we consider the dependence of illumination only upon coordinate y .

The speckle pattern in the plane situated at a distance l from the diffuser represents a superposition of the interference fringes originating during light scattering by each pair of points at the diffuser. The following regularities will therefore be true for the picture observed onscreen.

1. Any two points spaced distance b apart form interference fringes with frequency $f = b/(\lambda l)$ (see expression (2.38)).
2. The thinnest fringes (i.e., the fringes with frequency $f_{\max} = B/(\lambda l)$) are formed by the endpoints of diffuser.
3. For each $b_k < B$ there are a great number of point pairs forming the fringes with frequency $f_k = b_k/(\lambda l)$; the number of pairs of such points is proportional to $B - b_k$.
4. The dependence of illumination upon fringe frequency is linear inasmuch as $(f_{\max} - f) \sim (B - b_k)$ (Fig. 2.12).

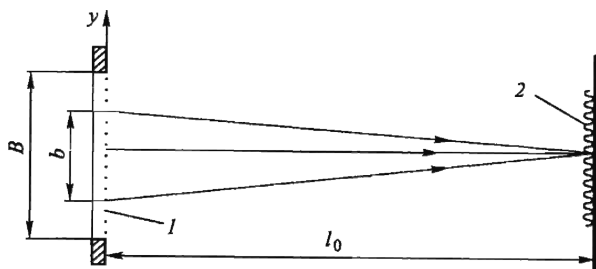
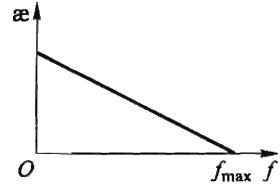


Fig. 2.11 Formation of speckles under laser light scattering by diffusively reflecting surface 1 – reflecting surface; 2 – fringes with frequency $f = b/(\lambda l)$

Fig. 2.12 Dependence of relative number α of the fringes involved in speckle formation upon spatial frequency f



According to the graph given in Fig. 2.12 the average frequency of fringes is

$$\langle f \rangle = \frac{1}{3} f_{\max} = \frac{1}{3} \frac{B}{\lambda l}. \quad (2.39)$$

Therefore, illumination distribution for a typical speckle pattern can be presented as follows,

$$I(y) \sim \cos^2 \left(\pi \frac{By}{3\lambda l} \right). \quad (2.40)$$

The speckle width b_s is taken to be the distance between points at which illumination falls by half. Taking this into consideration it follows from (2.39) and (2.40) that for the typical speckle

$$b_s \approx 1.5\lambda l/B. \quad (2.41)$$

If examining the object with a lens or other system-forming image, a uniformly illuminated diffuse surface may be thought of as a disc whose diameter is equal to lens diameter D . In the case when the image is formed at a distance l from the lens we obtain

$$b_s \approx 1.5\lambda l/D$$

More rigorous treatment fulfilled in [25] gives like correlation:

$$b_s \approx 1.22\lambda l/D.$$

If the system-forming image is focused by a lens on the relatively remote plane then it may be assumed that $l \approx F$ (where F is the lens focal length). Thereby

$$b_s \approx 1.22\lambda F/D. \quad (2.42)$$

Here $F/D = f$ is the numerical aperture of the lens. Allowing for the parameters of optical systems used in actual practice, the width of the speckle can be estimated. For example, using a helium–neon laser ($\lambda = 632.8 \text{ nm}$) it is between 4 to 100 μm .

2.2.3 Measurement of Tangential Displacements of Quasi-Planar Objects by Speckle Photography Technique

The speckle pattern recording geometry in the speckle photography technique is shown in Fig. 2.13. The surface of the object being studied is illuminated by a beam of coherent light impinging on the surface at a certain angle φ . A lens of diameter D with focal length F forms the surface image in the photographic layer plane.

The image of the object under study formed in the photographic layer plane is modulated by the random pattern of speckles whose average diameter can be estimated according to formula (2.42).

With displacement of the object in the direction of axis Oy by magnitude Δy the relative phase for each beam involved in formation of the speckle remains intact. The picture of speckles in the photographic plate plane in this direction will have displacements of magnitude $M\Delta y$ where M is the magnification of the optical system. It is evident that the displacement of speckles does not depend upon illumination angle φ .

To measure displacement of object points, in common with holographic interferometry, the double-exposure method is applied: the first exposure is carried out for the unloaded object being studied, and the second exposure after its loading.

If certain point $P_j(x, y)$ at the surface of the object being studied is shifted by magnitude $|\Delta_p| > b_s$ then two identical speckle pictures spaced $M|\Delta|$ apart take place on the developed photographic plate in the vicinity of this point. In principle the distance $M|\Delta|$ on the developed photographic plate for each pair of speckles can be measured by way of microscopic examination.

The alternative (and considerably better) method for measuring such displacements is coherent optical treatment of the photographic plate. For this purpose the zone of the point $P_j(x, y)$ vicinity is illuminated by a convergent laser beam formed by a lens with focal length F (Fig. 2.14a). The width of the laser beam is equal to 1 to 2 mm. As a result, the fringes with cosine illumination distribution are formed in the back focal plane of the lens (Fig. 2.14b). It occurs because each pair of appropriate speckles acts as a pair of identical sources of coherent light forming Young's fringes.

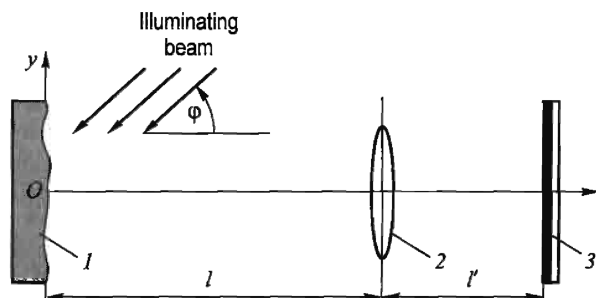


Fig. 2.13 Geometry of recording with using double-exposure speckle photography 1 – object plane; 2 – lens; 3 – image plane

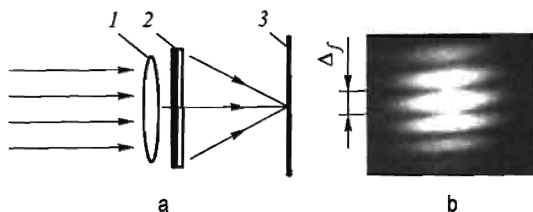


Fig. 2.14 Schematic of displacement measurement by method of double-exposure photography (a) and Young's fringes obtained with transillumination of a photographic plate (b)

Interpretation of the obtained interference pattern is evident: the fringes are oriented perpendicular to displacement vector $\mathbf{u} \equiv \Delta$ and the distance between them, according to (2.38), is in inverse proportion to the module. If in the transillumination zone of the photographic plate by the laser beam the distance between speckle pairs is equal to Δ , then the distance between the fringes will constitute $\Delta_f = \lambda F / \Delta$. Therefore, the displacement in the object point under consideration

$$\Delta = \frac{\lambda F}{M \Delta_f}. \quad (2.43)$$

For studying displacements of all points in the plane of the object being studied the sequential scanning of its image should be conducted. Application of present-day methods for digital image processing allows computerizing the process of displacement vector determination in the given points or cross-sections of the object being studied.

2.3 Electronic Speckle Pattern Interferometry

Using correlation speckle interferometry the requirements for resolution ability of the recording medium are considerably lower than for holographic interferometry. It is associated with the fact that in the first case there is a need to provide resolution of only the speckle pattern rather than the fine texture fringe arising in the hologram as a result of interference between the reference and object waves. As noted above, the sizes of the speckles lie within the range 4–100 μm . Therefore a standard television camera or other recording video system can be used along with photography to record the speckle pattern and thus the speckle correlation fringes. In this connection the method is also referred to as electronic digital speckle pattern interferometry (EDSPI).

The procedure for determination of intensity correlation in EDSPI is performed with the help of video signal addition and subtraction. Subtraction of video signals is carried out in the following way. The video signal corresponding to the speckle pattern of an undisplaced object in the image plane is fixed with the help of a video camera or charge-coupled device (CCD) matrix. This signal enters the electronic

storing device. Then the object is loaded. The video signal is derived in the same manner as for an unloaded object and is subtracted from the signal recorded in memory, filtered, and presented in digitized form.

One essential advantage of the EDSPI method is an opportunity to examine the dynamic fringe pattern directly on the display screen bypassing the intermediate stages of photographic record, accurate photographic plate adjustment, and so on.

2.3.1 Formation of Correlation Fringes

The basis for correlation speckle pattern interferometry methods [4, 25, 35, and others] is the addition of the speckle fields formed during illumination of the body by a laser light source with a reference wave. Another speckle field, the usual plane wave, or a spherical wave can be used as such a wave. The illumination distribution in the resultant speckle pattern obtained in this way will depend upon the relative phase shift of the fields being added. For studying the deformed state of the object by the EDSPI technique, as before, the method of double-exposure holographic interferometry is applied. The displacement of the surface of the object conditioned by its loading leads to a change in phase of the object's speckle field and, consequently, to illumination in the resultant speckle pattern.

In Fig. 2.15a the schematic is shown for determination of the displacement vector normal component by the speckle interferometry technique. The plane wave radiated by the laser light source impinges on the beamsplitter 3, is reflected from it and directed perpendicular to the diffusively reflecting surface 2 of the object being studied. After transmission through objective lens 5 the focused image of the object surface modulated by "subjective" speckles is obtained at photographic plate 6 (or another information carrier). To create the reference wave, the plane wave passed

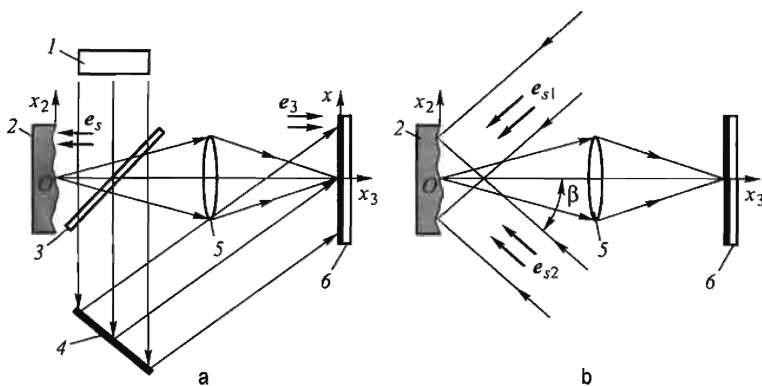


Fig. 2.15 Schematics of determining normal (a) and tangential (b) components of displacement vector by method of correlation speckle interferometry 1 – laser; 2 – object; 3 – beamsplitter; 4 – diffusive mirror; 5 – objective lens; 6 – photographic plate

through the beamsplitter is directed immediately to photographic plate 6 with the help of diffusive mirror 4.

The light flux impinging on plane ξ, χ of the photographic plate can be presented as follows,

$$E = B \exp(-i\varphi_1), \quad (2.44)$$

where $B(\xi, \chi)$, $\varphi_1(\xi, \chi)$ are the amplitude and phase of the wave reflected from the object in the initial state (for the first exposure). It should be noted that B and φ_1 are random functions.

The reference wave impinging on plane ξ, χ is

$$E_R = B_R \exp(-i\varphi_2), \quad (2.45)$$

where B_R and φ_2 are the amplitude and phase of the reference wave that are also random functions.

Let us determine the illumination distribution in the image plane:

$$\begin{aligned} I_1 &= \text{Re } |E + E_R|^2 = \text{Re } |[B \exp(-i\varphi_1) + B_R \exp(-i\varphi_2)] \\ &\quad \times [B \exp(i\varphi_1) + B_R \exp(i\varphi_2)]| \\ &= \text{Re } \left| B^2 + BB_R \exp(\varphi_1 - \varphi_2) + BB_R \exp(\varphi_2 - \varphi_1) + B_R^2 \right| \\ &= \left| B^2 + B_R^2 + BB_R \cos(\varphi_1 - \varphi_2) + iBB_R \sin(\varphi_1 - \varphi_2) \right. \\ &\quad \left. + BB_R \cos(\varphi_2 - \varphi_1) + iBB_R \sin(\varphi_2 - \varphi_1) \right| \end{aligned}$$

or

$$I_1 = \varsigma_1 + \varsigma_2 + 2\sqrt{\varsigma_1 \varsigma_2} \cdot \cos \varphi, \quad (2.46)$$

where $\varsigma_1 = B^2$, $\varsigma_2 = B_R^2$, and $\varphi = \varphi_1 - \varphi_2$ are random variables.

Correlation (2.46) describes the speckle pattern corresponding to the unloaded state of the object. The illumination distribution in the image plane taking place after object loading (for the second exposure) can be presented as

$$I_2 = \varsigma_1 + \varsigma_2 + 2\sqrt{\varsigma_1 \varsigma_2} \cdot \cos(\varphi + \delta), \quad (2.47)$$

where δ is the phase change due to object deformation.

Let us determine the correlation function $P(\delta)$ for two random functions I_1 and I_2 :

$$P(\delta) = \frac{\langle I_1 I_2 \rangle - \langle I_1 \rangle \langle I_2 \rangle}{\sqrt{(\langle I_1^2 \rangle - \langle I_1 \rangle^2) (\langle I_2^2 \rangle - \langle I_2 \rangle^2)}}, \quad (2.48)$$

In the case at hand

$$\begin{aligned}
 \langle I_1 I_2 \rangle &= \langle (\varsigma_1 + \varsigma_2 + 2\sqrt{\varsigma_1 \varsigma_2} \cdot \cos \varphi) [\varsigma_1 + \varsigma_2 + 2\sqrt{\varsigma_1 \varsigma_2} \cdot \cos(\varphi + \delta)] \rangle \\
 &= \left\langle \varsigma_1^2 + 2\varsigma_1 \varsigma_2 + \varsigma_2^2 + 2\varsigma_1 \sqrt{\varsigma_1 \varsigma_2} \cdot \cos \varphi + 2\varsigma_2 \sqrt{\varsigma_1 \varsigma_2} \cdot \cos \varphi \right. \\
 &\quad \left. + 2\varsigma_1 \sqrt{\varsigma_1 \varsigma_2} \cdot \cos(\varphi + \delta) + 2\varsigma_1 \sqrt{\varsigma_1 \varsigma_2} \cdot \cos(\varphi + \delta) \right. \\
 &\quad \left. + 4\varsigma_1 \varsigma_2 \cos \varphi \cos(\varphi + \delta) \right\rangle
 \end{aligned} \tag{2.49}$$

Because $\langle \cos \varphi \rangle = 0$ and $\langle \cos(\varphi + \delta) \rangle = \langle \cos \varphi \cos \delta - \sin \varphi \sin \delta \rangle = 0$ at $\delta \rightarrow 0$, from (2.49) we obtain

$$\begin{aligned}
 \langle I_1 I_2 \rangle &= \left\langle \varsigma_1^2 + 2\varsigma_1 \varsigma_2 + \varsigma_2^2 + 4\varsigma_1 \varsigma_2 \cos \varphi \cos(\varphi + \delta) \right\rangle \\
 &= \left\langle \varsigma_1^2 + 2\varsigma_1 \varsigma_2 + \varsigma_2^2 + 4\varsigma_1 \varsigma_2 \cos \varphi (\cos \varphi \cos \delta - \sin \varphi \sin \delta) \right\rangle \\
 &= \left\langle \varsigma_1^2 + 2\varsigma_1 \varsigma_2 + \varsigma_2^2 + 4\varsigma_1 \varsigma_2 \cos^2 \varphi \cos \delta \right\rangle.
 \end{aligned}$$

Taking into consideration that

$$\left\langle \cos^2 \varphi \right\rangle = \frac{1}{\pi} \int_0^\pi \cos^2 \varphi d\varphi = \frac{1}{2},$$

we find finally

$$\langle I_1 I_2 \rangle = \left\langle \varsigma_1^2 + 2\varsigma_1 \varsigma_2 + \varsigma_2^2 + 2\varsigma_1 \varsigma_2 \cos \delta \right\rangle. \tag{2.50}$$

Values I_1 , I_2 , and φ are independent variables, therefore they can be averaged:

$$\langle I_1 \rangle \langle I_2 \rangle = \langle \varsigma_1 + \varsigma_2 \rangle \langle \varsigma_1 + \varsigma_2 \rangle = \langle \varsigma_1 + \varsigma_2 \rangle^2. \tag{2.51}$$

The statistical properties of speckles were examined by Goodman [36]; the average value of the square of illumination was demonstrated by him to be equal to double the average illumination value quadratically; that is,

$$\left\langle I^2 \right\rangle = 2 \langle I \rangle^2. \tag{2.52}$$

Let us determine the denominator in expression (2.48):

$$\sqrt{(\langle I_1^2 \rangle - \langle I_1 \rangle^2)(\langle I_2^2 \rangle - \langle I_2 \rangle^2)} = \langle I_1 \rangle \langle I_2 \rangle = \left\langle \varsigma_1^2 + 2\varsigma_1 \varsigma_2 + \varsigma_2^2 \right\rangle. \tag{2.53}$$

Allowing for correlations (2.50)–(2.53), Eq. (2.48) takes the form:

$$P(\delta) = \frac{\langle \zeta_1^2 + 2\zeta_1\zeta_2 + \zeta_2^2 + 2\zeta_1\zeta_2 \cos \delta \rangle - \langle \zeta_1^2 + 2\zeta_1\zeta_2 + \zeta_2^2 \rangle / 2}{\langle \zeta_1^2 + 2\zeta_1\zeta_2 + \zeta_2^2 \rangle}.$$

Considering that $\langle \zeta_1 \rangle = \langle \zeta_2 \rangle = \langle \zeta \rangle$ we have finally

$$P(\delta) = \frac{1 + \cos \delta}{2}. \quad (2.54)$$

From (2.54) it follows that intercorrelation between illuminations I_1 and I_2 is equal to the unit at

$$\delta = 2\pi n, \quad (2.55)$$

and to zero at

$$\delta = (2n + 1)\pi, \quad (2.56)$$

where n is an integer number.

Thus, the change in the correlation function of the speckle pattern leads to formation of the fringe pattern; where expression (2.55) describes the whitish fringe formation condition and expression (2.56) describes the dark fringe formation condition. The resulting fringes are referred to as *fringes of speckle correlation* or *correlation fringes*.

2.3.2 Measurement Designs for Separate Components of the Displacement Vector

Let us assume that $\mathbf{u}(u_1, u_2, u_3)$ is the displacement vector of an arbitrary point at the body surface, where u_1, u_2, u_3 are the components of vector \mathbf{u} in the directions of axes Ox_1, Ox_2 , and Ox_3 , respectively. Let us introduce the following notations (see Fig. 2.15a): \mathbf{e}_S is the unitary vector in the direction of illumination of an arbitrary surface point; \mathbf{e}_3 is the unitary vector in the observation direction. It should be noted that when using a long-focus objective it is believed that $\mathbf{e}_3 = \text{const}$ for all points of the surface. With an allowance for agreed notations and according to (2.18), the expression for phase difference takes the form:

$$\delta = \frac{2\pi}{\lambda} (\mathbf{e}_3 - \mathbf{e}_S) \cdot \mathbf{u}. \quad (2.57)$$

To measure normal displacements u_3 let us avail ourselves of the optical schematic shown in Fig. 2.15a. In the Cartesian coordinate system $Ox_1x_2x_3$ (axis Ox_1 is perpendicular to the figure plane) vector components $\mathbf{e}_3, \mathbf{e}_S$, and \mathbf{u} have the following values,

$$\mathbf{e}_3 = (0, 0, 1); \quad \mathbf{e}_S = (0, 0, -1); \quad \mathbf{u} = (u_1, u_2, u_3). \quad (2.58)$$

Then expression (2.57) takes the form:

$$\delta = \frac{4\pi}{\lambda} u_3. \quad (2.59)$$

Allowing for (2.55) and (2.56) we obtain the following expression for the normal vector component,

$$u_3 = \frac{\lambda n}{2}$$

for whitish correlation fringes, and

$$u_3 = \frac{\lambda(2n + 1)}{2}$$

for dark correlation fringes.

The optical arrangement for finding the tangential component of a displacement vector is given in Fig. 2.15b. In this case the surface of the object under study (plane Ox_2x_3) is illuminated by two plane waves incident at equal angles in relation to axis Ox_1 . The surface image speckle pattern is formed by adding two speckle patterns corresponding to two vectors \mathbf{e}_{S1} and \mathbf{e}_{S2} . Making allowance for (2.57), we obtain the following expressions for δ_1 and δ_2 .

$$\delta_1 = \frac{2\pi}{\lambda} (\mathbf{e}_3 - \mathbf{e}_{S1}) \cdot \mathbf{u}; \quad \delta_2 = \frac{2\pi}{\lambda} (\mathbf{e}_3 - \mathbf{e}_{S2}) \cdot \mathbf{u}.$$

Having expressed the vectors in terms of their projections on axes Ox_1 , Ox_2 , and Ox_3 we obtain

$$\delta = \frac{4\pi}{\lambda} u_2 \sin \beta. \quad (2.60)$$

Therefore, the expressions for determining the tangential component of the displacement vector takes the form:

$$u_2 = \frac{\lambda n}{2 \sin \beta}$$

for whitish correlation fringes and

$$u_2 = \frac{\lambda(2n + 1)}{2 \sin \beta}$$

for dark correlation fringes.

2.3.3 Electronic Digital Speckle Pattern Interferometry

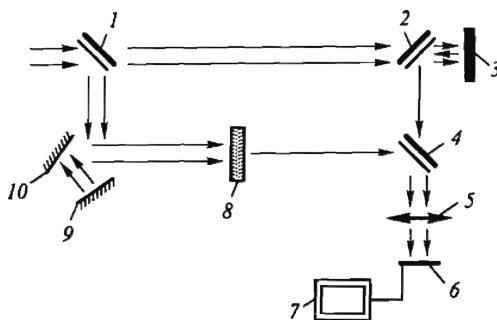
Let us consider an optical arrangement for determination of normal displacement fields by the EDSPI method based on the Mach–Zehnder interferometer (Fig. 2.16).

In an electronic speckle interferometer the initial plane wave is divided by plane-parallel plate 1 into object and reference beams. The first beam passing through semitransparent mirror 2 illuminates the specimen being studied 3. The wave diffusively reflected by its rough surface is directed by mirror 2 through plane-parallel plate 4 to output objective 5. The second beam circumscribing the loop with the help of mirrors 9 and 10 (for matching in interferometer arm lengths) hits on diffuser 8, a glass plate with one matte surface. The reference wave (with speckle pattern) coincides with the object wave by dint of plate 4 (here to create the reference wave the matte glass plate is used that somewhat simplifies the practical realization of the EDSPI method). The receiver in the form of matrix 6 coupled with computer 7 is installed in the image plane of objective 5, common for specimen and diffuser.

The procedure for determining the normal displacement pattern of a deformed object by the EDSPI method consists of recording in the form of computer files containing discrete digitized information about two (before and after loading) random illumination fields in the receiver plane and in their subsequent elementwise subtraction. Each file contains the interference sum of spatially superposed speckle patterns corresponding to the object and reference wave.

Both random functions of illumination are correlated (i.e., their difference tends to zero) with an ensemble of image points corresponding to the points of the object where its displacement constitutes the integer number of half-waves of the laser radiation used. Each such ensemble of points forms a sequent dark fringe at the subtractive video image reproduced on the computer display.

Fig. 2.16 Basic circuit arrangement of electronic speckle interferometer 1, 4 – plate glasses; 2 – mirror; 3 – specimen; 5 – objective lens; 6 – CCD matrix; 7 – computer; 8 – diffuser; 9, 10 – mirrors



2.3.4 Displacement Measurements by Digital Correlation Speckle Photography and Digital Holographic Interferometry Method

As noted above, the fundamental concept of measuring displacements in correlation speckle photography is finding conformity between two data arrays of speckle field distribution recorded by a digital detection unit for different states of the

object (before and after displacement). The mathematical procedure amounts to computation of data cross-correlation within the spatial dimensions of the recorded image. In the presence of speckle shift owing to the displacement of object points, the maximum cross-correlation function also shifts by the magnitude due to this displacement.

In the general case the algorithm for calculating the correlation function using a numerical procedure is determined by the following expressions.

$$P(d_x, d_y) = \int_{-\infty}^{\infty} \int_{-\infty}^{\infty} I_1(x, y) I_2(x + d_x, y + d_y) dx dy, \quad (2.61)$$

$$\bar{P}(d_x, d_y) = \Phi^{-1}\{\Phi[I_1(x, y)]^* \Phi[I_2(x + d_x, y + d_y)]\}$$

where $I_1(x, y)$ and $I_2(x + d_x, y + d_y)$ are the recorded intensities of the optical signal for two states of the object being studied, d_x and d_y are the shift in directions x and y , and $\bar{P}(d_x, d_y)$ is the correlation using the Fourier transform, where $\Phi(\dots)$ and $\Phi^{-1}(\dots)$ are the direct and inverse transformations. Both expressions in (2.61) are equivalent to each other, however, the second expression is very convenient in numerical techniques because it is realized using the fast Fourier transformation and essentially decreases the total quantity of computations.

In expression (2.61) we have the algorithm for finding the correlation function for two subimages taken from the speckle patterns corresponding to two different states of the object being studied. Scanning the whole data array allows the displacement of all points on the object surface to be calculated (Fig. 2.17).

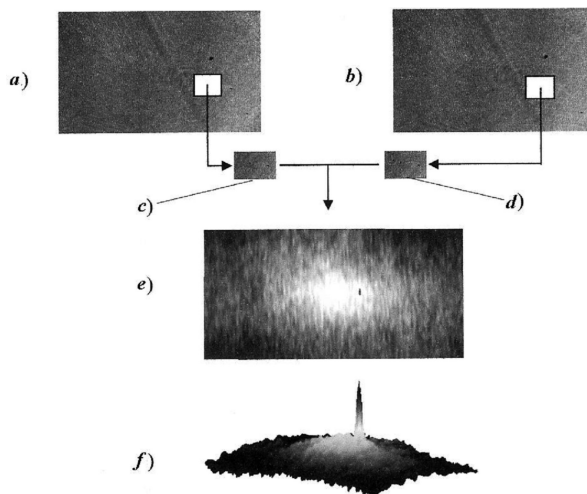


Fig. 2.17 Digital processing of speckle patterns: (a), (b) speckle patterns corresponding to two object states; (c), (d) zones of digital processing; (e) results of correlation function calculation; (f) after digital processing

The method discussed above, as a rule, is applied for measuring the displacements in the object plane because the correlation properties of the speckle are very sensitive to the displacements in the plane and considerably less sensitive to the displacements in the direction of observation. It is easy to understand by virtue of the fact that the speckles can be correlated only with themselves, and with their shift in the plane, the region of speckle overlap decreases markedly, but almost does not change in the perpendicular direction. When measuring the displacements normal to the object surface, the digital holographic interferometry technique offers definite advantages over the method of correlation speckle interferometry.

In the last few years the methods for image recording and processing where CCD cameras are applied as a recording medium have commonly been used in holographic interferometry. As a rule, the geometry for recording a focused image hologram with limited aperture is used (Fig. 2.18).

Intensity distribution due to interference between object and reference beams is recorded and digitized by the matrix of the CCD camera. For correct hologram digitization we must fulfill the Nyquist theorem condition, reasoning from pixel size ΔX and their number which places restrictions on spatial frequency and, as a consequence, on angle $\beta_{\max} = \lambda/2\Delta X$ between the object and reference beams [37]. For example, for a high-resolution camera 2048×2048 pixels with pixel size $\approx 9 \mu\text{m}$ for

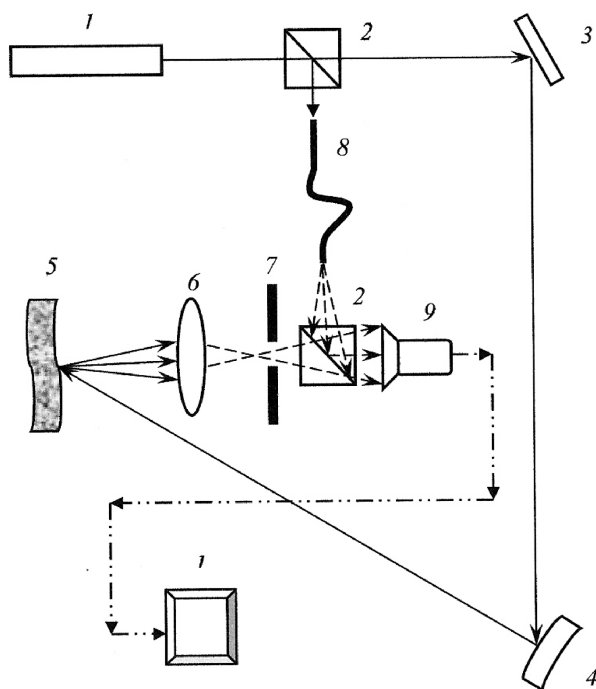


Fig. 2.18 Hologram recording geometry using digital camcorder 1 – laser; 2 – beam divider; 3 – mirror; 4 – spherical mirror; 5 – object being studied; 6 – lens; 7 – aperture; 8 – fiber optic with reference beam; 9 – CCD camera; 10 – computer

wavelength $\lambda = 532 \text{ nm}$ $\beta_{\max} \approx 1.7^\circ$. For recording geometries with digital cameras it is necessary to restrict not only the angle between the reference and object waves, but also, following from relation (2.42), the dimensions of the object beam itself. The restriction on the object field is performed by the aperture placed between the object and recording system. This aperture restricts the radiation frequency spectrum and defines the speckle size which should be taken into consideration because of the limited resolving power of the CCD camera. After image recording and digitizing, the procedure of calculating the object wave phase is carried out, and after recording two or more holograms and calculating their phases the construction of an interferogram is possible. The most widely applied method uses Fourier transforms.

As noted in Sect. 2.1.1 the intensity of illumination recorded by the CCD camera is determined by the relation:

$$I(x, y) = |E_{01} + E_R|^2 = \{B(x, y) \exp[i\varphi(x, y)] + A \exp(i\gamma)\} \times \{B(x, y) \exp[-i\varphi(x, y)] + A \exp(-i\gamma)\}.$$

By applying the Fourier transform to this expression we are led to the following expression,

$$\Phi(I) = \Phi |E_R|^2 + \Phi |E_{01}|^2 + E_R E_{01} \Phi\{\exp[-i(\gamma - \varphi)]\} + E_R E_{01} \Phi\{\exp[i(\gamma - \varphi)]\}. \quad (2.62)$$

In Fig. 2.19 the Fourier transform of intensity $I(x, y)$ using a rectangular diaphragm can be seen. The central area corresponds to the intensity constituent of the source and object field.

Filtration of the part of the transformation derived, namely, the object area containing the data about phase, and fulfillment of the inverse Fourier transformation

$$\Phi^{-1}\{E_R E_{01} \Phi\{\exp[i(\gamma - \varphi)]\},$$

reconstruct the wave of the form $AB \exp[i(\gamma - \varphi)]$.

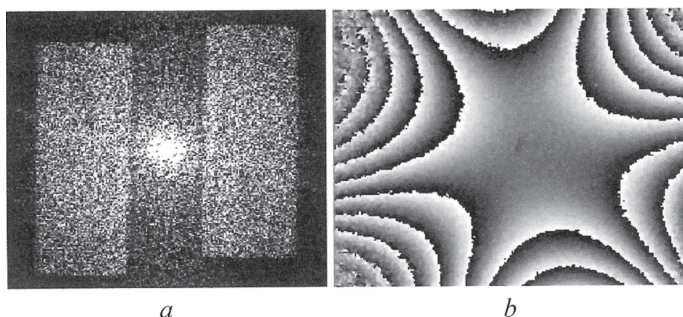


Fig. 2.19 Image processing using the digital holography method: (a) Fourier transformation recorded by digital camera; (b) characteristic distribution of interference fringes obtained by digital method (research in disk oscillations at resonant frequency)

The phase difference between the initial state of the object and any other state, for example, in the case of phase deformation $E_{02} = AB \exp\{i[\gamma - (\varphi + \Delta\varphi)]\}$ can be calculated based on the expression:

$$\operatorname{tg}(\Delta\varphi) = \operatorname{tg}(\varphi_{02} - \varphi_{01}) = \frac{\operatorname{Im}(\varphi_{01}) \times \operatorname{Re}(\varphi_{02}) - \operatorname{Im}(\varphi_{02}) \times \operatorname{Re}(\varphi_{01})}{\operatorname{Im}(\varphi_{01}) \times \operatorname{Im}(\varphi_{02}) + \operatorname{Re}(\varphi_{01}) \times \operatorname{Re}(\varphi_{02})}. \quad (2.63)$$

Formula (2.63) defines the function of the phase difference distribution depending on the initial and final object states [38]. It should be noted that the method stated for phase reconstruction based on Fourier transformation is not the only one. There are a number of simpler and less time-consuming calculation methods, for example, the three- or four-pixel method [39], however, as a rule they require more complicated recording geometry and also they do not always allow the method being considered to be used for research in dynamic processes.

It should be noted that tangential fringe distribution is obtained at the final interferogram (Fig. 2.19b). In such a distribution the direction of change in intensity of the interference fringe is connected unequivocally with the deformation direction. The said circumstance facilitates interferogram interpretation and construction of the surface of the object deformed state, whereas for classic cosine distribution of interference fringes (see (2.10), (2.20), and (2.54)) it is impossible to determine the direction of displacement.

As in classic holographic interferometry, in digital methods the connection between phase difference and displacement vector is expressed by correlation (2.18).

In coherent optical methods the interference fringe processing is always connected to the necessity of determining the minima of intensity in the presence of optical noise, the cause of which is coherent illumination of diffusively reflecting surfaces and, consequently, the random character of recorded speckle patterns.

With the aim of excluding the influence of the noise specified in obtaining the pattern of intensity distribution by the speckle interferometry method, Shambless and Broadway [40] proposed using the fast Fourier transform in a digital filter algorithm. The digital filter performs the procedure for smoothing initial information during the process of which ultraharmonics are truncated, and inverse transformation (Fourier) of the data filtered from optical noise allows their smoothing to be obtained. In the first research using the specified approach, layer-by-layer scanning of speckle patterns was performed; that is, Fourier transformation was used as a linear filter. The results of inverse transformation essentially depend upon the number of terms of series n (into which the functions expand under digital processing) being taken into account with direct (n_1) and inverse (n_2 , $n_2 < n_1$) transformations. In this connection in the course of data processing the magnitude \bar{n} optimal for experimental data of the type being considered was determined empirically based on analysis of filtered patterns [41].

The use of digital technologies in coherent optical methods represents natural development and more convenient realization of coherent optical methods, however, they also open up fresh opportunities for complete automatic performance of measurements from recording moment to construction of the displacement field.

Analysis of the information obtained is performed by mathematical methods of image processing. In digital holographic interferometry the stage of recording holographic images for different object states is separated in time which allows the analysis of the optical signal to be performed combinatorially or separately.

Present-day coherent optical methods allow the measurements of rather complicated mechanical processes to be carried out; high-speed processes, resonant multifrequent oscillations, nonsteady mechanical states of objects, and also measurements at the macro- and mezzo-level [27, 42–45] can be assigned to these processes.

In conclusion it should be noted that in cases when all three components of the displacement vector are to be determined, the optimal way for problem solution is the application of digital holography in combination with digital correlation speckle photography: either for compensation of point displacement in the direction perpendicular to observation and separation of phase difference as a result of complex displacement (vibration, deformation) [46] or, vice versa, in order to exclude influence of complex movement [47].

2.4 Examples of Practical Application for Coherent Optical Methods

2.4.1 Analysis of Object Surface Displacement During Static Deforming

The method of holographic interferometry is extensively used in practical research, in particular for measuring displacements under static loading of full-scale construction components or their laboratory models. Determination of displacement vector fields is based on solving linear equations of type (2.20) for the given ensemble of points at the body area being studied. Column-vector coordinates in the right-hand side of the equations are the functions of fringe orders in just the same arbitrary point of the object defined on at least three interferograms with linearly independent sensitivity vectors $\mathbf{K}_j = (\mathbf{ps} + \mathbf{po})_j, j = 1, 2, \dots, m$ ($m \geq 3$) recorded simultaneously in separate interferometers. To identify just the same points when observing the object in different foreshortenings, the special coordinate grids preliminarily applied at its surface are used. As a rule, construction of a global measurement system supposes use of one illuminating wave ($\mathbf{e}_s = \text{const}$) and several observation directions with noncoplanar vectors \mathbf{e}_j . In so-called multihologram interferometers the waves scattered by a deformed body in several directions are recorded at different spatially spaced holograms with their own reference beams. Construction of such sufficiently unmanageable measurement systems is coupled with considerable technical difficulties.

When studying small-scale objects or limited areas of relatively large structures the approach is more efficient in accordance with which the waves scattered by the body are registered at one hologram recorded according to Denisjuk's scheme [22] (Fig. 2.20).

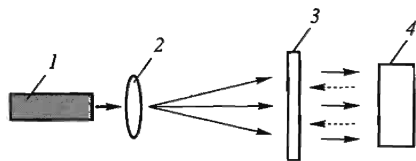


Fig. 2.20 Optical arrangement of hologram recording in counterpropagating beams 1 – laser; 2 – beam expander (microscope objective); 3 – photographic plate (hologram); 5 – object

Here the object wave is the part of the initial wave passed through the photographic plate and diffusively reflected by the body surface in the inverse direction. Hitting again on the photographic plate it interferes with the initial wave coming from the opposite direction which fulfills the role of a reference wave. Thus in this case the difference in the path of the waves involved in hologram formation is equal to the doubled distance between the photographic plate and object and, consequently, for the purpose of high-grade recording of interference structure this distance must be minimal when possible. It should be noted that the holograms recorded according to Denisyuk's scheme can be reconstructed in achromatic light. If in the recording of such a hologram the photographic plate is installed at a short distance from the object then during reconstruction its virtual image can be observed in a relatively great spatial angle.

For subsequent interferogram processing usage of an illuminating wave with directing vector $e_s(0, 0, -1)$, that is, orthogonal to the plane Oxy tangent to the object surface in the measurement point, is the most convenient. Observation and recording (e.g., photography) of interferograms are conducted from the points lying at the director circle of a circular cone with the axis coinciding with axis Oz (Fig. 2.21).

If cone height is sufficiently great then vectors e_j might be reckoned as constant for all object areas under study. Each observation position is characterized by a common angular opening of cone 2ψ and azimuth direction angle of position θ_j of the appropriate point on the circle. Equations of type (2.20) take on the form:

$$u_1 \cos \theta_j \sin \psi + u_2 \sin \theta_j \sin \psi + u_3(1 + \cos \psi) = \lambda N_j, \quad (2.61)$$

$$j = 1, 2, \dots, m,$$

where N_j is the function of fringe orders in the object point under consideration.

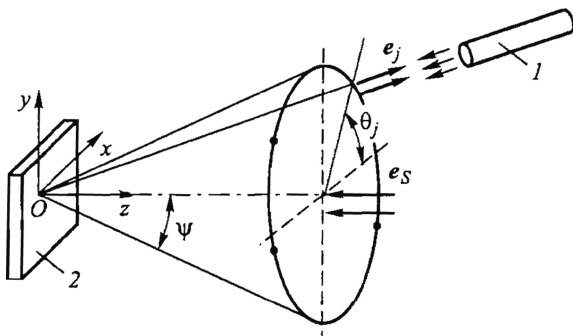


Fig. 2.21 Observation system under measurement of object displacement fields by reflective hologram method 1 – laser; 2 – hologram

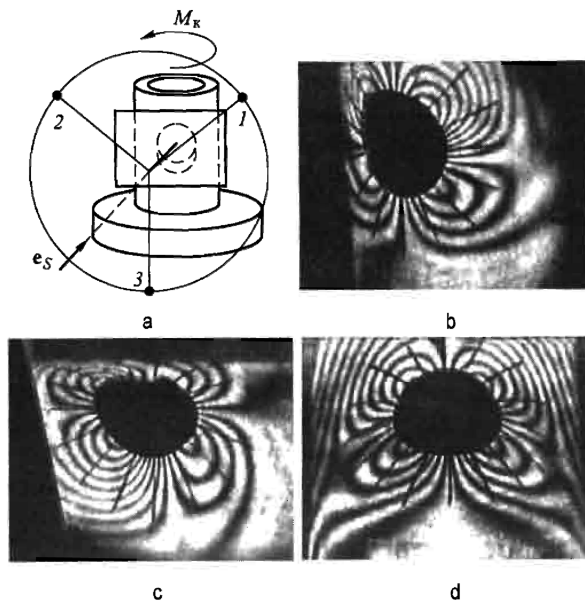


Fig. 2.22 Schematic of research in cylindrical shell with circular cutout (a) and interferograms derived from observation points 1 (b), 2 (c), and 3 (d)

With the number of observation points $m > 3$ Eq. (2.61) can be solved by the least squares method which contributes to improving the accuracy of the final results.

In Fig. 2.22 the example of using the research approach described for torsional deformation of a cylindrical shell with circular cutoff is given.

In particular, in Fig. 2.19(b)–(d) the holographic interferograms are fixed in the system of observation with $\psi = 45^\circ$ from points $\theta_{1,2,3} = 30^\circ, 150^\circ$, and 270° , respectively. Determining the values (in the general case, nonintegral) of functions of fringe orders in points marking hole contours, and solving equation system (2.61) for each such point, the discrete distributions of separate constituents of the displacement vector can be constructed.

At this point the primary mathematical treatment stage of experimental information ends. The rest of the procedure is determined by the ultimate goals of the problem to be solved. So, after interpolation and differentiation of the dependences obtained for contour displacements it is possible to calculate local strain distributions and to estimate their concentration level.

2.4.2 Research in Overhead-Track Hoist Displacement by Speckle Photography Technique

As noted above, speckle photography has certain advantages over holographic interferometry: less rigid requirements for mechanical stability of the information logging system, simplicity of optical arrangement, and also ease of result acquisition and interpretation.

Let us consider an example of a practical speckle photography application for research in displacements in an object surface plane. The analysis of displacements is only a part of integrated SSS study for a typical “boxlike” overhead-track hoist widely used in present-day carrying and lifting machines. The study was conducted using a 3-D model made of optically sensitive material ED-20-M in scale 1:10; it included two stages.

At the first stage displacements of the object were determined by the speckle photography method. Inasmuch as to obtain a laser speckle pattern the object surface must be diffusively reflecting, one thin coating of white was applied to the model (with the help of a standard pulverizer).

At the second stage the stresses in the most loaded zones of the model were measured by the freezing method. Some results of the study are presented in Fig. 2.23.

In Fig. 2.23a the right half of an overhead-track hoist model and also a schematic of its fixation and loading are shown. The left half of the model after freezing was cut into slices for measuring stresses by the photoelastic technique. To determine displacements of the overhead-track hoist wall the coherent optical treatment of a developed photographic plate by a convergent beam was used (see (2.2.3)).

Let us analyze the results of the speckle photography treatment presented in Fig. 2.23b–d. In Fig. 2.23b Young’s fringes are absent and, consequently, displacement of point A is close to zero. In Figs. 2.23c,d it can be seen that as the distance from the zone of overhead-track hoist fixation increases, the displacements also increase (as evidenced by the decrease in distance between Young’s fringes).

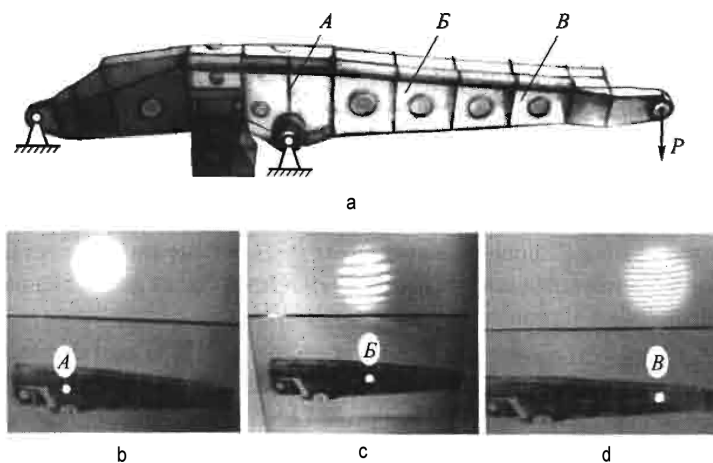


Fig. 2.23 Loading and fixing diagram of overhead-track hoist model (a) and research results by speckle photography (b)–(d)

2.4.3 Research in Characteristics of Material Deforming by EDSPI Method

The feasibility of high-precision recording of whole displacement fields makes application of holographic interferometry and EDSPI methods on experimental mechanics of materials attractive. With the help of these methods actual strain distribution at the entire surface of the object being tested can be determined without touching. A practically unlimited quantity of information allows statistical analysis to be used. The basic advantage of these methods is also the possibility of conducting qualitative and quantitative verification of compliance with the computational deforming model during the experiment including detection of loading errors (skewnesses, misalignments, etc.) and also specimen manufacturing defects.

Let us consider the special case of EDSPI application for materials testing under the conditions of pure bending with the aim of determining constants of elastic deformation [48]. In Fig. 2.24a the simplest experimental arrangement for measuring normal components of the displacement vector and a typical pattern of interference fringes arising under bending of the specimen in the form of a thin

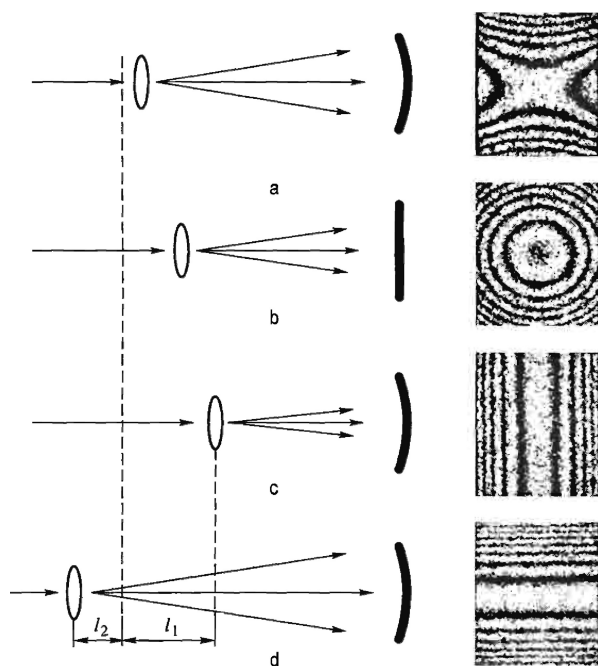


Fig. 2.24 Compensation method for measuring the principal curvature of a deformed surface under pure bending

rectangular plate are given. A quantitative interpretation of such an interferogram can be as follows. For normal displacements the correlation can be written:

$$w(x, y) = \frac{\chi_x x^2 + \chi_y y^2}{2} + R(x, y) = \frac{M}{EJ} (x^2 - \mu y^2) + Ax + By + C, \quad (2.62)$$

where χ_x, χ_y are the two main curvatures of the deformed specimen surface; $R(x, y)$ is the function characterizing actual displacement of the specimen as the rigid whole, $R(x, y) = Ax + By + C$; M is the bending moment; and I is the inertia moment of the specimen cross-section.

Elastic constants E and μ of a material can be determined according to the values of the coefficients of Eq. (2.62), quadratic terms found on the basis of the least squares method according to displacements $w(x, y)$ measured at the interferogram. However, in many respects the determination of Eq. (2.62) coefficients based directly on the optical compensation of specimen deformation (in the strict sense, curvature) is more effective. Origination of the interference pattern can be caused by both displacement of the object proper and change in the conditions of its illumination.

It may be shown that variation in the curvature of a wavefront is provided by a simple shift of the microscope objective forming the given wave along axis Ox by magnitude l (Fig. 2.24b). (A shift in direction to the specimen is taken as a negative shift). The observed fringe pattern represents a system of coaxial circles and corresponds formally to the fictive specimen bending deflections described by the expression

$$w_0 = \frac{\chi_0}{2}(x^2 + y^2), \quad (2.63)$$

where χ_0 is the coefficient of the additional field.

With small shifts ($l \rightarrow 0$) the change in front curvature χ_f for illuminating the wave constitutes $\Delta\chi_f = R^{-1} - (R + l)^{-1} \cong l/R^2$, where R is the initial distance between the microscope objective and specimen. No variations in optical lengths of light beams occur at the section of the object wave path between the specimen and observation point (not shown in the figure), therefore correlation $\chi_0 = 2\Delta\chi_f = 2l/R^2$ is true.

The procedure of compensation changes is as follows. Originally the initial fringe pattern for bending moment M is visualized on a real-time basis, and also the condition $A = B \equiv 0$ is provided by special technical means. Then the increase (in absolute magnitude) in the coefficient χ_0 determined by expression (2.63) is pursued by uniform movement of the microscope objective. At one point the interferogram acquires the form of rectilinear fringes parallel to one of the main axes of curvature for a deformed surface (Fig. 2.21c). This state corresponds to the point of compensation of the main curvature of one specimen. In this case summarized field $w + w_0$ is a function of only parameter y whence it follows that condition $\chi_x = -\chi_{01} = 2l_1/R^2$, ($l_1 < 0$) is fulfilled. Therefore, measuring l_1 we actually determine χ_x , where the scale of values l can be graduated directly in strains. It

should be noted that although the bending deflections themselves do not exceed ten micrometers, the movement of the microscope objective as an output parameter of the compensation interferometer constitutes millimeters; that is, it is recorded reasonably accurately even by the usual means of measuring linear dimensions.

To record other main curvatures the direction of the microscope objective movement is reversed (Fig. 2.24d). The moment of compensation corresponds to condition $\chi_y = -\chi_{02} = -2l_2/R^2$, ($l_2 > 0$). Thus, elastic constants of specimen material can be calculated with the help of simple correlations:

$$E = \frac{2M}{\chi_x J} = -\frac{MR^2}{l_1 J}, \quad \mu = -\frac{\chi_y}{\chi_x} = -\frac{l_2}{l_1}. \quad (2.64)$$

The schematic of a compensation speckle interferometer for determining mechanical characteristics is given in Fig. 2.25.

The basis of the measurement system is the speckle interferometer with two diffuse beams [49]. The initial plane wave is divided by plane-parallel plate 1 into an object wave and reference wave. The first wave passing sequentially through movable 2 and fixed 3 objective lenses and semitransparent mirror 4 illuminates the specimen being studied 5. The wave diffusively reflected by its rough surface is directed by semitransparent mirror 4 through plane-parallel plate 6 to output objective 7. The second wave circumscribing the loop with the help of mirrors 11 and 12 (for matching in interferometer armlengths) hits on diffuser 10, a glass plate with one matte surface. The reference wave being received in a speckle pattern coincides with the object wave by dint of plate 6. The receiver in the form of CCD matrix 8 coupled with computer 9 is installed in the image plane of the objective 7 common for specimen and diffuser. An additional phase shift is performed by three-dimensional movement of movable lens 2. Translation of the lens is accompanied by identical motion of the point source of spherical waves S , and also a small

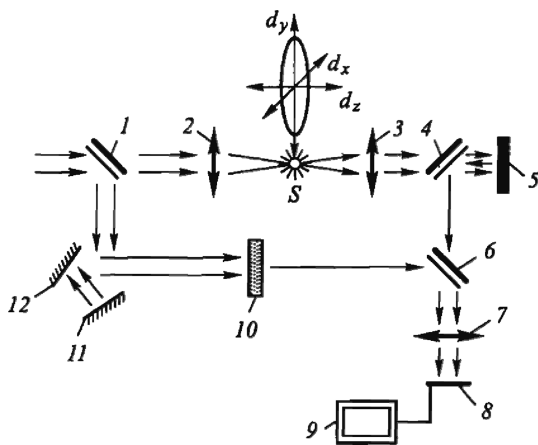


Fig. 2.25 Schematic of compensation electronic speckle interferometer 1, 6 – plate glasses; 2, 3 – movable and fixed lenses; 4 – semitransparent mirror; 5 – specimen; 7 – objective lens; 8 – CCD matrix; 9 – computer; 10 – diffuser; 11, 12 – mirrors

quantity of the movement of the parameters M, A , and B in Eq. (2.62) are determined independently by its components d_x, d_y, d_z (see Fig. 2.25).

It should be noted that the method can be used for studying the mechanical behavior of structural materials under bending not only in elastic but also in the elastoplastic range of deforming for both the uniaxial and two-axial stressed state. In prospect the given method can be extended to solving the problems of determination of deformation characteristics under the conditions of elastoplastic deformations and creep on the basis of mathematical treatment of the experimental information obtainable with stepwise change in load.

The example of EDSPI method application for research in residual stresses is considered in Chap. 4.

2.4.4 Research in Vibration Characteristics for Construction Components Interacting with Liquid Media

Among the topical issues arising at the intersection of deformable solid mechanics and hydromechanics research in vibration characteristics of construction components in liquid media is of major importance. Often use of experimental modeling techniques for such aims has no alternative (from initial database creation for substantiation of theoretical models to accumulation of practical results for verification of calculation algorithms and programs).

Holographic interferometry holds a most unique position among the means for experimental investigation in vibrations of construction components. Its prime advantage is the possibility of visualization and digital description of the whole field of displacements at the surface of the object being studied that enables interpretation of primary experimental information with maximum correctness and, consequently, enhances credibility of obtainable results.

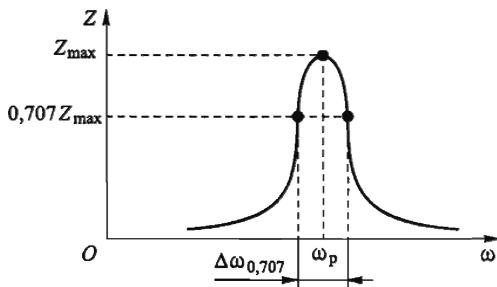
The holographic method of vibratory displacement recording can also be used for determination of the oscillation decrement dependent upon internal friction of the object proper as well as upon dissipative properties of the ambient medium. The basis for this is a known approach to estimating damping constant δ according to the relative width of the resonance peaks at amplitude frequency response (AFR) [50]:

$$\delta = \frac{\pi \Delta\omega_{0,707}}{\omega_r}, \quad (2.65)$$

where $\Delta\omega_{0,707}$ is the width of the resonance peak at level 0,707 Z_r, Z_r is the maximal amplitude of oscillations at the moment of observable resonance, and ω_r is the resonance frequency (Fig. 2.26).

Both amplitude displacements and their derivatives can be considered as a recordable response $Z(x, y)$ of the construction to vibration loading. In particular, under the conditions of bending oscillations of thin structures the first derivatives of deflection functions characterize distribution of local turns of deformable surface elements and

Fig. 2.26 Determination of logarithmic decrement of oscillations according to AFR parameters



the second derivatives, their acquired curvature or their increment. It makes it possible to avoid influencing the results of displacements of the object being studied as a rigid whole and also eliminates the factor related to suppleness of construction component fixation. It is evident that in such a case there is a need to record the field of amplitude displacements at the whole object surface being studied or, at any rate, in the vicinity of the given point that can also be realized with the help of the holographic time-averaging method.

During studying vibrations of bodies in liquid media the object is placed in a special chamber with transparent walls or viewing windows filled with liquid. Then the interferometer itself is arranged out of the chamber.

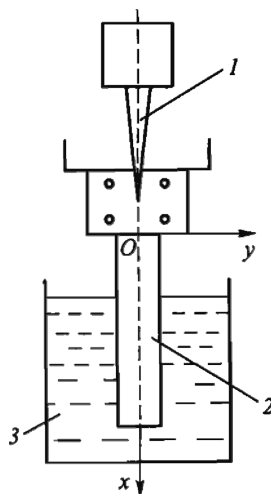
The important condition for obtaining adequate primary information is also three-dimensional uniformity and stationarity of the optical properties of the liquid. It should be noted that one cause of change in the refraction index can be locally periodic change in pressure in the liquid medium produced by the oscillatory motion of the solid body itself. The effect of this factor requires, in the strict sense, special research.

To measure vibration characteristics of objects in a liquid medium custom-made rigid tanks with glass viewing windows 6 mm in thickness were used [51]. The design of the experimental facility excluded undesirable vibration loading of the tanks themselves. Water (density $\rho = 1.0 \text{ g/cm}^3$; dynamic viscosity $\eta = 0.1 \text{ Pa} \cdot \text{s}$), mineral oil PMS-100 ($\rho = 1/\text{g/cm}^3$; $\eta = 10 \text{ Pa} \cdot \text{s}$), and glycerin ($\rho = 1.26 \text{ g/cm}^3$; $\eta = 1150 \text{ Pa} \cdot \text{s}$) were used as liquid media. Comparison of research results in the air and in the specified liquid media permitted the evaluation of the effect of ambient density and viscosity on vibration characteristics of the object under study.

Loading was performed with the help of the local vibration action device based on piezoceramic transducers. The point of load application was located in the area of rigid fixation of the object being studied, that is, at the zone where nodal lines for any resonant form of its oscillations pass. In this case the natural oscillations of the object were caused by a deformation wave in the material with essentially small amplitudes of displacements of the vibrator exciter working member. As a source of coherent radiation the helium–neon laser with a capacity 15 MW generating coherent radiation with wavelength $\lambda = 0.6328 \mu\text{m}$ was used.

To elaborate the procedure the stationary vibrations of the test specimen in the form of a cantilever-fitted thin aluminum plate with dimensions of $120 \times 52 \times 3 \text{ mm}$

Fig. 2.27 Fixation and vibration excitation diagram of the specimen in the form of a cantilevered plate in liquid medium 1 – exciter projector; 2 – specimen; 3 – trough filled with liquid

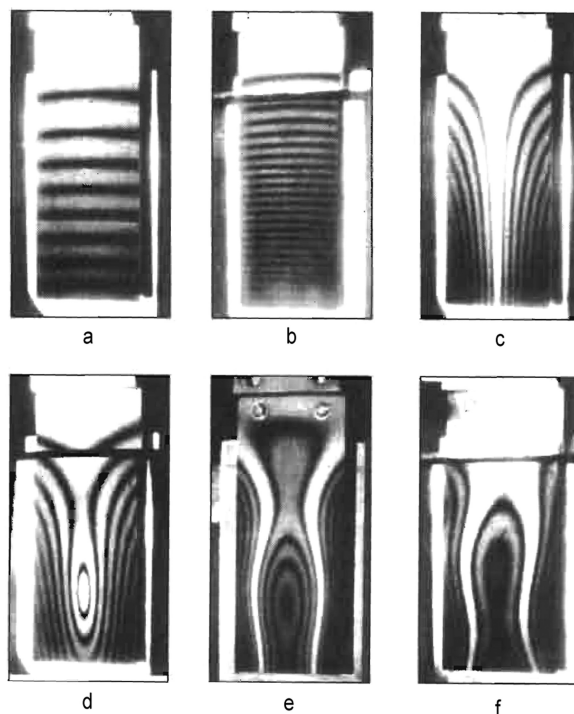


were studied in the air and water (Fig. 2.27). A vertically oriented plate was immersed into a glass trough filled with water. In the course of the experiment the natural frequencies and oscillation modes of the plate were measured in the air and also in the water upon condition of plate remoteness from the rigid fixed screen and in the case when the screen was installed behind the plate at a distance of 1.5 mm.

In Fig. 2.28 the selected typical interference patterns of equal amplitude displacements recorded by the time-averaging method under the conditions of resonance oscillations are shown. To denote oscillation modes (k ; l) of the plate, in general, the numbers corresponding to the quantity of horizontal (k) and vertical (l) nodal lines are used. It was established that certain natural modes are of similar form during exciting plate oscillations in the air and liquid media, for example, pure bending modes (1;0), (2;0), (3;0); flexural-torsional mode (3;1), and so on. At the same time certain modes under the conditions of oscillations in liquid took on peculiar distinctions, for example, alteration of torsional (1;1) and flexural-torsional (2;1) oscillation mode.

To determine the damping factor for the isolated plate immersed in water the appropriate AFR were plotted. As response parameters, the amplitude of normal displacements at the center of the plate and local values of the first and second derivatives of deflection function $Z(x, y)$ in relation to longitudinal specimen axis Ox obtained by mathematical treatment of interferograms were considered. After real-time registration of the resonance frequency for the oscillation mode, the hologram recording was conducted by the time-averaging method for a number of closely spaced excitation frequencies. On the basis of the mathematical treatment of interferograms in accordance with correlation (2.29) the field of oscillation amplitudes was determined for each frequency. Turns and curvature in the given point (for bending oscillations of thin structures) were determined by differentiation of the interpolation function with respect to the spatial coordinates. As a result AFR was plotted as dependence of the accepted response Z upon excitation frequency.

Fig. 2.28 Interference patterns corresponding to plane oscillation modes (1;0) (a), (b), (1;1) (c), (d) and (1;2) (e), (f) a, c, e – in the air, $\omega = 172$; 829 and 6277 Hz; b, d, f – in water, $\omega = 72$; 482 and 4029 Hz



Approximation of experimental points by appropriate functions was carried out using the least squares method. Credibility and accuracy of results as well as the possibility itself of executing the given procedure were determined by the quantity of the points used, that is, the number of fringes of the interferogram. The interference patterns characterizing amplitude displacements of the plate in liquid obtained at different excitation frequencies are shown in Fig. 2.29.

In such a case the damping factor constituted 0.065.

The procedure approved and debugged at the plates was used for research on the effect of liquid media on vibration characteristics of the tube bundle (Fig. 2.30) representing a full-scale segment of the heat exchanger of a power plant. The segment consisted of nine tubes 10.5 mm in diameter, 0.5 mm in wall thickness, and with relative lattice spacing 1.24.

The examples of the interferograms obtained are given in Fig. 2.31 and the dependence of natural frequencies upon the kind of ambient medium in Fig. 2.32.

In accordance with the results of experiments, the AFC of object oscillations in the air and liquid in the region of resonance frequencies can be plotted. The example of such an AFC is given in Fig. 2.33.

Thus, reasoning from analysis of the effect of liquid media on the vibration characteristics of construction components it is possible to build mathematical models ensuring an adequate description of the interaction processes between tube bundles

Fig. 2.29 Interferograms of amplitude displacements under research in plate oscillations in water at resonance frequency 3817 Hz (flexural mode (4;0)) (a) and at near-resonant excitation frequencies 3750 (b) and 3710 Hz (c)

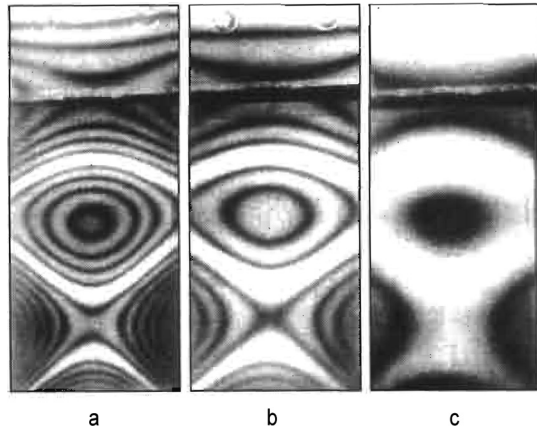
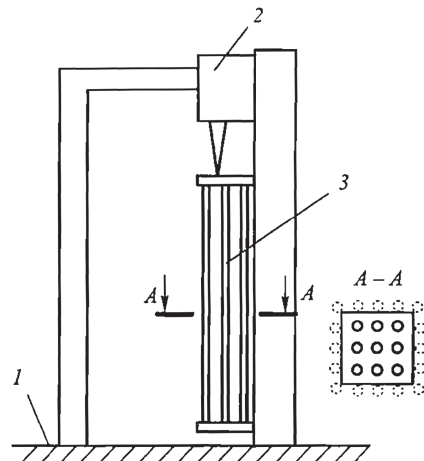


Fig. 2.30 Schematic of experimental facility for research in vibration characteristics of tube bundle
1 – interferometer base;
2 – vibration exciter;
3 – tube bundle



and liquid media of different density and viscosity and permitting us to take into consideration both the actual properties and design peculiarities of the object being studied.

2.4.5 Nondestructive Testing of Materials

The methods of electronic speckle interferometry and holographic interferometry are successfully applied for nondestructive testing of materials and products for the detection of defects that are impossible to identify by visual examination [23, 36, and others].

The testing is based on registration of object surface displacements under the action of minute loads. The presence of defects stipulates irregularity of obtainable

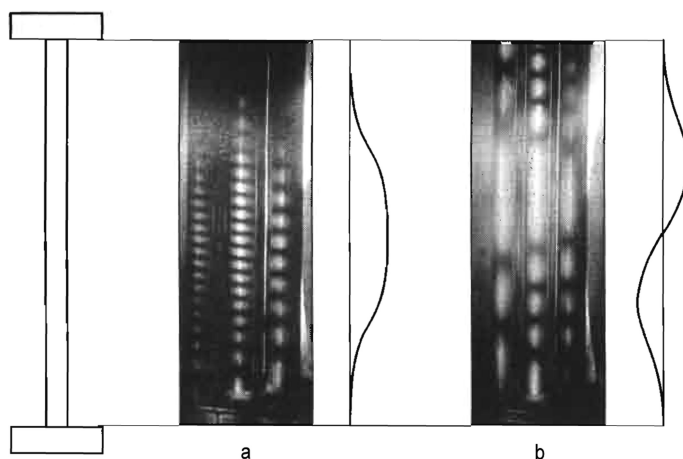
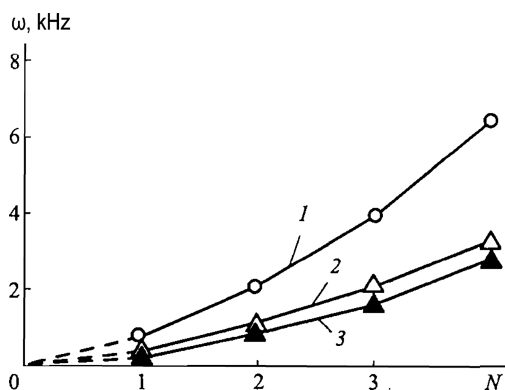


Fig. 2.31 Interferograms of tube bundle amplitude displacements obtained during research in oscillations at the first and second natural frequencies equal to 338 (a) and 1050 Hz (b)

Fig. 2.32 Effect of ambient medium on natural frequencies of tube bundle oscillations (N – order of natural frequency) 1 – air; 2 – water; 3 – glycerin



interference patterns that allow the defect position area to be determined and also in most cases their sizes and types (holes, cracks, etc.) to be evaluated. Thus, the presence of internal subsurface defects can be evaluated even if the zone of their effect on the SSS character includes the component surface area under examination.

In the course of research one should take into account that the defects can be revealed only in the case where their sizes are not less than the minimum distance between interference fringes. Otherwise the defect will not markedly affect the fringe geometry.

To create surface displacements of the object being studied various types of loads are used, the choice of which depends upon the kind of material, design features, and defect character. The simplest loading method is heating of the component (as a rule, by tens of degrees Celsius). However, thermal loading is effective only

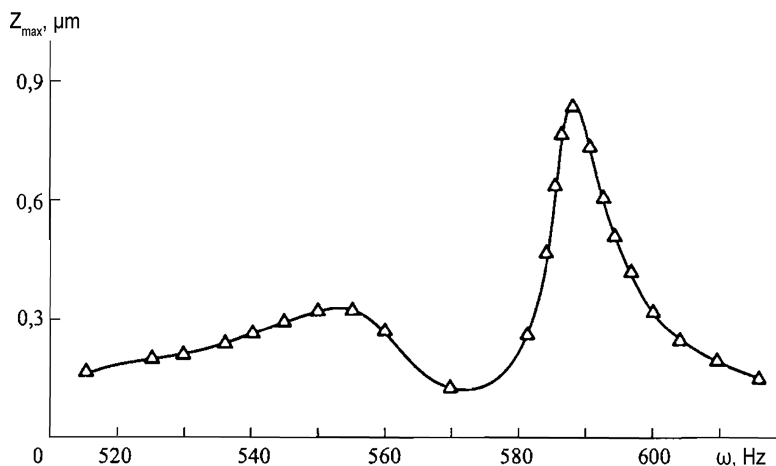


Fig. 2.33 Amplitude-frequency characteristic obtained during research on a single tube by oscillations in PMS-100 according to flexural mode (1;0)

for research on nonhomogeneous materials (or products of them) and composite constructions in as much as even during uniform heating the stresses conditioned by distinguishing between thermal expansion coefficients of different material or component constituents arise in them. For the products made of homogeneous isotropic materials, mechanical static or vibration loading should be used.

Examples of nondestructive testing by the holographic interferometry technique are shown in Fig. 2.34. At an interference pattern of normal displacements obtained by heating a fuel cylinder made of boron–aluminum (boron fibers in an aluminum matrix) the zone of irregularity (discontinuity) in the interference fringes is visible and demonstrates the presence of a horizontal crack (see Fig. 2.34a).

The interference pattern shown in Fig. 2.34b is obtained by heating the honeycomb panel used in aircraft construction. The external surface of the panel is made of a thin multilayer material joined to the honeycomb element of the aluminum alloy necessary for an increase in the material's bending stiffness. The irregularity

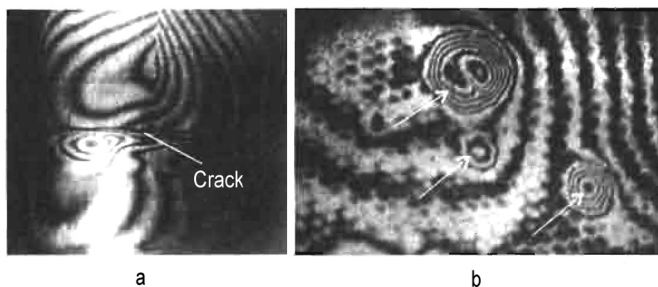


Fig. 2.34 Zones of irregularity in interference patterns due to presence of defects

regions in the interference fringes (shown in the figure by arrows) allow the absence of cohesion zones between the multilayer material and honeycomb element to be defined.

* * *

Coherent optical techniques and, especially, EDSPI should be considered as the most promising methods in experimental mechanics of deformable solids. At the present time these methods are growing rapidly along the following lines.

Modernization of instrumentation

Development of new methodological approaches in the field of solving fundamental issues of the mechanics of deformable solids

Widening the scope of effective application

Certainly, development of the specified lines occurs in the presence of strong interrelation between them

With respect to instrumentation development the major issue is the miniaturization of equipment with a simultaneous increase in both the volume of information and its processing rate, as well as in the power of the coherent radiation source (and with a simultaneous reduction in its cost). It provides a way for essential widening of the scope of practical tasks to be solved including pursuing research under factory conditions and even in the field environment. At the present time the compact EDSPI-based installations are made for research in material properties in the field and for research in residual stresses. Pulse holography has been developed along the same lines where the application of powerful lasers makes it possible to obtain interference displacement patterns at exposures up to 10^{-7} s; that is, the capability to examine dynamic processes is realized.

Integrated combination of deformed object state recording on the basis of coherent optical methods with computer technologies and computational analysis on the basis of FEM offers formidable challenges to the development of mechanics of deformable solids along the most diverse lines. Let us dwell on several of them.

The EDSPI technique presents the possibility of monitoring deformation processes over a wide range of rates by stepwise change in loading parameters that can be used as the basis for analyzing nonlinear characteristics of material deformation with the most diverse properties (including present-day composite materials). Evolution of the ways of obtaining deformation parameters of such materials requires elaboration of models and test specimens for their determination and, on the other hand, methods for mathematical processing of experimental information.

Recent capabilities of solving deformable body mechanics problems by numerical FEM-based procedures, in particular, analysis of the SSS, vibration characteristics, stiffness, and so on, have no principal limitations. However, it is evident that in many cases when the question is the complex nonlinear processes of material straining, interaction between object and ambient medium (e.g., viscous liquid), and also nonlinear links, the formulation of mathematical models allowing these processes to be described adequately is possible only on the basis of experiment. Coherent

optical methods are the most effective way to verify calculated procedures and programs under the refining adequacy of the proposed model (rather than robustness of the assumed computation algorithm).

Admittedly, application of the EDSPI method for research in residual stresses has to be regarded as a cutting-edge trend. It concerns the development of new approaches to analyzing nonuniform fields of residual stresses as well as the application of the EDSPI method and the appropriate equipment for practical research (see Chap. 4).

In conclusion we dwell on the issue following from the character of experimental information derived by coherent optical methods. The case in point is the determination of object deformations according to the displacement patterns obtained. As a rule, the problem boils down to the procedure of differentiation (single or double) of the data about displacement distribution at the surface of the object being studied. In principle, its solution is possible on the basis of very diverse methods: finite differences, spline approximation, least squares, and so on. Apparently, at the present time the use of experimental displacement distribution as initial information for SSS calculation has to be regarded as the simplest and most effective approach to the determination of deformations. At the same time it should be noted that at the stage of designing construction components to conduct the calculations of strains and stresses on a FEM basis it is preferable, if necessary, to use various experimental methods for refinement of one or another task parameter.

Interference-optical Methods of Solid Mechanics

Razumovsky, I.A.

2011, XIII, 180 p., Hardcover

ISBN: 978-3-642-11221-8